Draft version August 8, 2014
Preprint typeset using LaTeX style emulateapj v. 5/2/11

arXiv:1408.1406v1 [astro-ph.HE] 6 Aug 2014

ROCHE-LOBE OVERFLOW SYSTEMS POWERED BY BLACK HOLES IN YOUNG STAR CLUSTERS: THE IMPORTANCE OF DYNAMICAL EXCHANGES

Michela Mapelli & Luca Zampieri[1]

Draft version August 8, 2014

ABSTRACT

We have run 600 $N-$body simulations of intermediate-mass (~ 3500 M$_\odot$) young star clusters (SCs) with three different metallicities ($Z = 0.01$, 0.1 and 1 Z$_\odot$). The simulations include the dependence of stellar properties and stellar winds on metallicity. Massive stellar black holes (MSBHs) with mass > 25 M$_\odot$ are allowed to form through direct collapse of very massive metal-poor stars ($Z < 0.3$ Z$_\odot$). We focus on the demographics of black hole (BH) binaries that undergo mass transfer via Roche lobe overflow (RLO). We find that 44 per cent of all binaries that undergo an RLO phase (RLO binaries) formed through dynamical exchange. RLO binaries that formed via exchange (RLO-EBs) are powered by more massive BHs than RLO primordial binaries (RLO-PBs). Furthermore, the RLO-EBs tend to start the RLO phase later than the RLO-PBs. In metal-poor SCs ($0.01 - 0.1$ Z$_\odot$), > 20 per cent of all RLO binaries are powered by MSBHs. The vast majority of RLO binaries powered by MSBHs are RLO-EBs. We have produced optical color-magnitude diagrams of the simulated RLO binaries, accounting for the emission of both the donor star and the irradiated accretion disk. We find that RLO-PBs are generally associated with bluer counterparts than RLO-EBs. We compare the simulated counterparts with the observed counterparts of nine ultraluminous X-ray sources. We discuss the possibility that IC 342 X-1, Ho IX X-1, NGC 1313 X-2 and NGC 5204 X-1 are powered by a MSBH.

Subject headings: black hole physics – stars: binaries: general – galaxies: star clusters: general – X-rays: binaries – methods: numerical – stars: kinematics and dynamics.

1. INTRODUCTION

Most stars ($\sim 70 - 90$ per cent) are believed to form in star clusters (SCs, e.g. Lada & Lada 2003; Porras et al. 2003; Parker & Goodwin 2007; Portegies Zwart, McMillan & Gieles 2010; Silva-Villa & Larsen 2010; Gvaramadze et al. 2012; Kharchenko et al. 2012; Kharchenko et al. 2013; see also Bressert et al. 2010 and Gieles, Moeckel & Clarke 2012 for a possible issue). The percentage of SCs that remain bound after the evaporation of gas (i.e. after the first few Myrs) is more uncertain: it may be as low as ~ 5 per cent and as high as ~ 30 per cent, and it might also depend on the environment (e.g. Bastian 2008; Silva-Villa & Larsen 2010; Goddard, Bastian & Kennicutt 2010; Gieles & Portegies Zwart 2011). The fraction of SCs that survive for > 100 Myr is likely lower (~ 5 per cent, Lada & Lada 2003).

Thus, most progenitors of stellar black holes (BHs) form in SCs, and a number of BHs spend the first part of their life in a young SC, before being possibly ejected into the field. This is crucial to understand the formation and evolution of X-ray binaries.

In fact, dense young SCs are collisional stellar systems: their two-body relaxation timescale is shorter than (or comparable to) their lifetime (e.g. Portegies Zwart, McMillan & Gieles 2010). For example, the half-mass relaxation timescale for a SC with total mass $M_{\rm TOT} \sim 10^4$ M$_\odot$ and half-mass radius $r_{\rm hm} \sim 1$ pc (such as NGC 3603 and Trumpler 14) is $t_{\rm rlx} \sim 20$ Myr (e.g. Portegies Zwart & McMillan 2002). This implies that close encounters between stars and binaries (three-body encounters), and even triples or multiple systems (e.g. Leigh & Geller 2013) play an important role in the overall dynamical evolution of a SC, as well as in the fate of single objects (e.g. Hills 1975). During a three-body encounter, the binary and the single star exchange energy (e.g. Heggie 1975). This alters the orbital properties of the binary, and may induce recoil on the center of mass of the involved bodies (e.g. Aarseth & Hills 1972; Hills & Fullerton 1980; Heggie & Hut 1993; Sigurdsson & Phinney 1993; Sigurdsson & Phinney 1995; Davies 1995; Colpi, Mapelli & Possenti 2003; Mapelli et al. 2005). Dynamical exchanges can also occur, i.e. three-body encounters during which the single star replaces one of the former members of the binary. The probability of an encounter to end up with a dynamical exchange is higher if the mass of the single star is equal or higher than the mass of one of the binary members (Hills 1989; Hills 1992).

These dynamical effects are crucial for the formation of BH binaries (i.e. binaries hosting at least one BH): a BH that was born single in the field will likely remain single forever, whereas a single BH in a collisional SC may acquire a companion through dynamical exchanges. Since the probability of exchange depends on the mass, this process will favor the formation of BH binaries hosting the most massive BHs in a SC (e.g. Hills 1976; Hills 1991). Mapelli et al. 2013 (2013, hereafter M13) studied the dynamical evolution of BHs in young SCs with various metallicity, and found that $20 - 25$ per cent of

[1] INAF-Osservatorio Astronomico di Padova, Vicolo dell'Osservatorio 5, I–35122, Padova, Italy; michela.mapelli@oapd.inaf.it

simulated BHs form from single stars and become members of binaries through dynamical exchange in the first 100 Myr of the SC life. This fraction rises to ~ 75 per cent if only the most massive BHs (> 25 M$_\odot$) are considered. Also, dynamical encounters induce a mass-transfer phase and the birth of an X-ray binary.

From an observational perspective, bright X-ray binaries and ultraluminous X-ray sources (ULXs, i.e. point-like non-nuclear X-ray sources with luminosity, assumed isotropic, $L_X > 10^{39}$ erg s^{-1}) are often associated with OB associations and with young SCs (e.g. Goad et al. 2002; Zezas et al. 2002; Liu et al. 2004; Soria et al. 2005; Ramsey et al. 2006; Terashima, Inoue & Wilson 2006; Abolmasov et al. 2007; Berghea 2009; Swartz, Tennant & Soria 2009; Tao et al. 2011; Grisé et al. 2011; Grisé et al. 2012; Bodaghee et al. 2012; Coleiro & Chaty 2013). This may indicate that the dynamics of the parent SC enhances the formation of bright X-ray binaries. In addition, a significant fraction of these bright X-ray sources are found to be slightly displaced (by few tens to hundreds of parsecs) from the closest young SC (Zezas et al. 2002; Kaaret et al. 2004; Berghea 2009; Rangelov et al. 2012; Poutanen et al. 2013; Berghea et al. 2013). This has been interpreted as a consequence of natal kicks (e.g. Sepinsky, Kalogera & Belczynski 2005; Zuo & Li 2010) and of dynamical recoil (e.g. Kaaret et al. 2004; Mapelli et al. 2011b).

Population synthesis simulations of field binaries provide valuable information about the demographics of X-ray binaries (e.g. Portegies Zwart, Verbunt & Ergma 1997; Hurley, Tout & Pols 2002; Podsiadlowski, Rappaport & Pfahl 2002; Podsiadlowski, Rappaport & Han 2003; Belczynski et al. 2004a; Belczynski, Sadowski & Rasio 2004b; Rappaport, Podsiadlowski & Pfahl 2005; Dray 2006; Madhusudhan et al. 2006, 2008; Belczynski et al. 2008; Linden et al. 2010), but do not take into account the effects of dynamics. The few studies of BH demographics in young SCs that include both stellar evolution and dynamics (e.g. Blecha et al. 2006; M13; Goswami, Kiel & Rasio 2014) highlight that the effects induced by dynamics (especially dynamical exchanges) cannot be neglected, even in the first 10 Myr of the young SC life. In particular, M13 is the first study of the dynamical evolution of BHs in young SCs that includes self-consistent recipes for the formation of massive stellar BHs (MSBHs, with mass $m_{\rm BH} > 25$ M$_\odot$) in metal-poor environments. In this paper, we adopt the same recipes as in M13, and we focus on the demographics of BH binaries that undergo Roche lobe overflow (RLO). We give particular attention to the formation pathways of RLO systems and to the properties of the donor star.

The paper is structured as follows. In Section 2, we briefly describe the method adopted for the simulations. In Section 3, we present the results, focusing on the formation pathways of BHs (Section 3.1), on the importance of dynamical exchanges for RLO binaries (Section 3.2), on the role of MSBHs (Section 3.3), on the properties of the donor stars (Section 3.4), and on the distribution of the simulated binaries in the color-magnitude diagram (CMD, Section 3.5). In Section 4, we discuss the main results and compare the simulated systems with the observed counterparts of some ULXs. In Section 5, we summarize the most relevant results and discuss future challenges for $N-$body simulations of SCs.

2. METHOD AND SIMULATIONS

The simulations have been done using the STARLAB public software environment (Portegies Zwart et al. 2001), which includes the KIRA direct-summation N-body integrator and the SEBA code for stellar and binary evolution (Portegies Zwart & Verbunt 1996; Portegies Zwart et al. 2001; Nelemans et al. 2001). The recipes for binary evolution adopted in this paper are the same as described in Portegies Zwart et al. (2001), while the recipes for stellar evolution are the same as described in M13 (see also Mapelli & Bressan 2013). In particular, SEBA was modified in M13, to include various effects of metallicity, as follows.

In M13, the metallicity dependence of stellar radius, temperature and luminosity was added to SEBA, using the polynomial fitting formulas by Hurley, Pols & Tout (2000). The recipes for mass loss by stellar winds were updated, by using the metal-dependent fitting formulas for main sequence (MS) stars provided by Vink, de Koter & Lamers (2001; see also Belczynski et al. 2010). Furthermore, we added an approximate treatment of stellar winds for luminous blue variable (LBV) stars and for Wolf-Rayet (WR) stars. A post-MS star becomes a LBV star if $L/{\rm L}_\odot > 6 \times 10^5$ and $10^{-5}\,(R/{\rm R}_\odot)\,(L/{\rm L}_\odot)^{0.5} > 1.0$, where L and R are the luminosity and the radius of the star, respectively (Humphreys & Davidson 1994). A LBV star loses mass by stellar winds at a rate $\dot{M} = f_{\rm LBV} \times 10^{-4}$ M$_\odot$ yr^{-1}, where $f_{\rm LBV} = 1.5$ (Belczynski et al. 2010). Naked helium-giant stars with zero-age MS (ZAMS) mass $m_{\rm ZAMS} > 25$ M$_\odot$ are considered WR stars (e.g. van der Hucht 1991), and lose mass by stellar winds at a rate[2] $\dot{M} = 10^{-13}(L/{\rm L}_\odot)^{1.5}\,(Z/{\rm Z}_\odot)^{\beta}$ M$_\odot$ yr^{-1}, where $\beta = 0.86$ (Hamann & Koesterke 1998; Vink & de Koter 2005; Belczynski et al. 2010).

A star with ZAMS mass $8 \leq m_{\rm ZAMS}/{\rm M}_\odot < 25$ undergoes supernova (SN) explosion by the end of its life and becomes a neutron star[3] (NS). The NS receives a natal kick randomly selected from the distribution $P(u) = \frac{4}{\pi}\frac{1}{(1+u^2)^2}$, where $u = v/\sigma$ (v is the NS velocity modulus and $\sigma = 600$ km s^{-1}, Hartman 1997).

Stars with ZAMS mass $m_{\rm ZAMS} \geq 25\,{\rm M}_\odot$ and final mass (i.e. the mass bound to a star immediately before the collapse) $m_{\rm fin} < 40$ M$_\odot$ undergo SN explosion and become a BH, because of fallback of material from the SN ejecta. The natal kick for a BH born by SN explosion is drawn from the same distribution as that of NSs, but scaled to $m_{\rm NS}/m_{\rm BH}$ (where $m_{\rm NS}$ is the typical NS mass, here approximately taken to be equal to 1.34 M$_\odot$).

Stars with final mass $m_{\rm fin} \geq 40$ M$_\odot$ collapse to a BH directly, without SN explosion (Fryer 1999). The mass of a BH born from direct collapse is very similar to $m_{\rm fin}$, since there are no ejecta. In particular,

[2] In this definition and throughout the text, we adopt ${\rm Z}_\odot = 0.019$.

[3] We assume that all stars with $8 \leq m_{\rm ZAMS}/{\rm M}_\odot < 25$ ($m_{\rm ZAMS} \geq 25\,{\rm M}_\odot$) become NSs (BHs), regardless of metallicity. The actual threshold is expected to depend on metallicity. On the other hand, our assumption is quite robust up to $Z \sim {\rm Z}_\odot$ (see e.g. figure 1 of Heger et al. 2003).

the mass spectrum of BHs born from direct collapse is the same as described in Fig. 1 of M13. Since our recipes of mass loss by stellar winds depend on metallicity (Vink, de Koter & Lamers 2001; Vink & de Koter 2005), metal-poor stars have higher values of $m_{\rm fin}$ than metal-rich stars with the same $m_{\rm ZAMS}$, and collapse to more massive BHs. BHs with mass up to ~ 40 (80) $M_\odot$ can form at $Z = 0.1$ (0.01) $Z_\odot$ by direct collapse of single stars. Furthermore, BHs born from direct collapse do not receive any natal kicks (Fryer et al. 2012).

In our simulations, BHs with mass > 25 $M_\odot$ are allowed to form even through merger of a BH or a NS with another star. We assume no mass loss during the merger (which is rather optimistic, e.g. Gaburov, Lombardi & Portegies Zwart 2010), since we do not have recipes for hydrodynamical treatment of the star-star mergers. BHs with mass ≥ 25 $M_\odot$ (which form either by direct collapse or by merger) are named massive stellar BHs (MSBHs, Mapelli et al. 2009; Mapelli et al. 2010; Mapelli et al. 2011a; Mapelli et al. 2011b; M13).

Finally, we recall that the stellar evolution recipes adopted in this work (Hurley, Pols & Tout 2000) are based on single-star evolution models, while recipes for binary evolution are the same as described in Portegies Zwart et al. (2001). Recipes for binary evolution include prescriptions for angular momentum loss by magnetic stellar wind and/or by gravitational wave radiation, tidal circularization, circularization by gravitational wave emission, mass transfer and Roche lobe filling, common envelope, and binary merger.

2.1. *Initial conditions and simulation grid*

In this paper, we describe the results of 600 $N-$body simulations of young SCs (200 with metallicity $Z = 0.01$ $Z_\odot$, 200 with $Z = 0.1$ $Z_\odot$, and the remaining 200 with $Z = 1$ $Z_\odot$). Each group of 200 simulations with the same metallicity is a different realization of the same SC model. We ran many different realizations of the same SC to obtain a sufficiently large sample of BH binaries and to damp stochastic fluctuations (each SC hosts $\sim 8-9$ BHs on average, see M13). Half of the simulations presented in this paper are the same as described in M13. The remaining simulations are new runs.

Each simulated SC is modelled as a spherical King profile with central dimensionless potential $W_0 = 5$ (King 1966) and $N_* = 5500$ stars (corresponding to an initial total mass $M_{\rm TOT} \sim 3000-4000$ $M_\odot$). Table 1 shows the main initial properties of the simulated SCs.

A primordial binary (PB) fraction $f_{\rm PB} = 0.1$ was adopted. This means that ~ 18 per cent of all stars in the simulated SCs are members of a binary system, since $f_{\rm PB}$ is defined as the number of PBs in each SC divided by the number of 'centers of mass' (CMs) in the SC (see Table 1 for details).

The mass of single stars was randomly drawn according to a Kroupa initial mass function (IMF, Kroupa 2001), with minimum mass $m_{\rm min} = 0.1$ $M_\odot$ and maximum mass $m_{\rm max} = 150$ $M_\odot$. The same procedure was adopted to select the mass of the primary member of a binary (i.e. the most massive member of a binary), while the mass of the secondary member (m_2) was drawn from a uniform distribution between $0.1\,m_1$ and m_1 (where m_1 is the mass of the primary). The initial semi-major axis a of a binary was chosen from a distribution $f(a) \propto 1/a$ (Sigurdsson & Phinney 1995; Portegies Zwart & Verbunt 1996). The minimum and the maximum allowed value of the semi-major axis are 1 $R_\odot$ and 10^5 $R_\odot$, respectively, but we discard systems whose periapsis is smaller than the sum of the radii of the two stars (Portegies Zwart, McMillan & Makino 2007). The maximum value of the semi-major axis is sufficiently large to include a number of soft binaries. The initial eccentricity e of a binary is randomly selected from a thermal distribution $f(e) = 2\,e$, in the $0-1$ range (Heggie 1975).

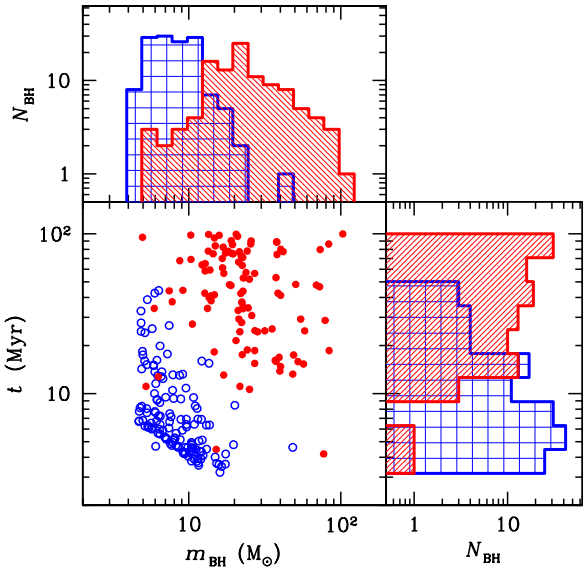

Figure 1. Main window: mass of the BHs that power a simulated RLO system versus the time when the RLO phase starts. Red filled circles: RLO-EBs (i.e. EBs that undergo RLO). Blue open circles: RLO-PBs (i.e. PBs that undergo RLO). The marginal histograms show the distribution of the masses of BHs that power RLO systems and the distribution of the times when the RLO phase starts ($t = 0$ is the beginning of the simulation). In both marginal histograms, the red hatched histogram (blue cross-hatched histogram) refers to RLO-EBs (RLO-PBs). In this plot, all the simulated SCs are shown, and we do not distinguish between different metallicities.

We integrate the evolution of these SCs for the first 100 Myr. We recall that the half-mass relaxation timescale for these SCs is $t_{\rm rlx} \sim 10\,{\rm Myr}\,(r_{\rm hm}/0.8\,{\rm pc})^{3/2}\,(M_{\rm TOT}/3500\,{\rm M}_\odot)^{1/2}$, where $r_{\rm hm}$ is the initial half-mass radius of the SC (in our simulations $r_{\rm hm} \sim 0.8-0.9$ pc). Thus, the core collapse timescale (Portegies Zwart & McMillan 2002) is $t_{\rm cc} \approx 3\,{\rm Myr}\,(t_{\rm rlx}/10\,{\rm Myr})$.

The properties of the simulated SCs ($M_{\rm TOT}$, $r_{\rm c}$ and $r_{\rm hm}$) match those of observed dense young SCs (e.g. the Orion Nebula Cluster, Portegies Zwart, McMillan & Gieles 2010; see also Hillenbrand & Hartmann 1998; Dias et al. 2002; Pfalzner 2009; Kuhn et al. 2012). Finally, our simulations do not account for the tidal field of the host galaxy. The effect of tidal fields will be added and discussed in forthcoming papers. In Section 4.2, we discuss some additional caveats concerning our choice of the initial conditions.

3. RESULTS

Table 1
Most relevant initial conditions.

Parameter	Values
W_0	5
N_*	5500
r_c (pc)	0.4
c	1.03
IMF	Kroupa (2001)
$m_{\rm min}$ ($M_\odot$)	0.1
$m_{\rm max}$ ($M_\odot$)	150
Z ($Z_\odot$)	0.01, 0.1, 1.0
$f_{\rm PB}$	0.1

Note. — *Notes.* W_0: central dimensionless potential in the King (1966) model; N_*: number of stars per SC; r_c: initial core radius; $c \equiv \log_{10}(r_t/r_c)$: concentration ($r_t$ is the initial tidal radius); IMF: initial mass function; $m_{\rm min}$ and $m_{\rm max}$: minimum and maximum simulated stellar mass, respectively; Z: metallicity of the SC; $f_{\rm PB}$: fraction of PBs, defined as the number of PBs in each SC divided by the number of 'centers of mass' (CMs) in the SC. In each simulated SC, there are initially 5000 CMs, among which 500 are designated as 'binaries' and 4500 are 'single stars' (see Downing et al. 2010 for a description of this formalism). Thus, 1000 stars per SC are initially in binaries.

Table 2
Summary of the formation pathways for simulated LBHs (i.e. only the BHs with $m_{\rm BH} < 25$ $M_\odot$).

Z ($Z_\odot$)	Single star	Star in PB	Star-star merger	BH-star merger
0.01	1310 (11)	127 (57)	118 (0)	15 (0)
0.1	1318 (17)	110 (45)	106 (2)	22 (0)
1.0	1432 (29)	98 (38)	131 (2)	30 (1)
All[a]	4060 (57)	335 (140)	355 (4)	67 (1)

Note. — *Notes.* Column 1: metallicity of the SC; column 2: number of simulated LBHs that are born from single stars; column 3: number of simulated LBHs that are born from stars in PBs (in column 3 we consider only the cases in which the PB does not merge before the formation of the BH; the cases in which the binary merges before the formation of the BH are listed in column 4); column 4: number of simulated LBHs that are born from the merger of two stars (in ~ 95 per cent of cases the two merging stars are two members of a PB); column 5: number of simulated LBHs that are born from the merger of a star and a BH.
The numbers within parentheses (in each column) refer to the number of LBHs that power RLO systems belonging to each formation pathway.
[a]'All' refers to the statistics of all runs without distinguishing between different metallicities.

Table 3
Summary of the formation pathways for simulated MSBHs (i.e. only the BHs with $m_{\rm BH} \geq 25$ $M_\odot$).

Z ($Z_\odot$)	Single star	Star in PB	Star-star merger	BH-star merger
0.01	218 (19)	18 (1)	17 (0)	42 (1)
0.1	194 (13)	8 (0)	11 (1)	40 (4)
1.0	0 (0)	0 (0)	10 (1)	27 (2)
All[a]	412 (32)	26 (1)	38 (2)	109 (7)

Note. — *Notes.* The same as Table 2 but for MSBHs.

3.1. *Formation pathways of BHs*

Tables 2 and 3 summarize the different formation pathways of simulated BHs, in the case of light BHs (LBHs, i.e. BHs with $m_{\rm BH} < 25$ $M_\odot$) and MSBHs (with $m_{\rm BH} \geq 25$ $M_\odot$), respectively.

Most LBHs come from single stars (~ 85 per cent), regardless of metallicity. Only $\sim 6-8$ per cent of LBHs originate from stars in PBs, and $\sim 7-8$ per cent form from the merger of two stars (the mergers occur mainly between two members of a PB). This is statistically consistent with the fact that ~ 18 per cent of stars are members of PBs in our simulations. Finally, $\sim 1-2$ per cent of LBHs come from the merger of a BH and a star. In the vast majority of cases the BH and the star were already members of a binary before merging, and most of these BH-star binaries were not PBs. In several cases, the formation of an unstable triple system triggers the BH-star merger (e.g. Leigh & Geller 2013).

The numbers within parentheses in Table 2 refer to the number of LBHs that power RLO systems belonging to each formation pathway. Remarkably, the majority of LBHs that power RLO systems come from PB members ($\sim 54-84$ per cent, depending on metallicity), even if only $\sim 6-8$ per cent of LBHs originate from stars in PBs.

Most MSBHs at low metallicity ($Z = 0.01$, 0.1 $Z_\odot$) come from the direct collapse of single stars ($\sim 74-77$ per cent), while no MSBHs form from single stars at high metallicity ($Z = 1$ $Z_\odot$), as a direct consequence of our stellar evolution models.

The percentage of MSBHs that form from stars in PBs is very low (0, 3 and 6 per cent at $Z_\odot$, 0.1 $Z_\odot$ and 0.01 $Z_\odot$, respectively). The reason is that mass-transfer and common-envelope phases in tight PBs cause either the PB to merge or the first BH to be much lighter than in case of a single-star progenitor (as already shown by Linden et al. 2010).

The percentage of MSBHs that form from the merger of two stars is very low at low metallicity (4 and 6 per cent at 0.1 $Z_\odot$ and 0.01 $Z_\odot$, respectively), while it is relevant at high metallicity (27 per cent at $Z_\odot$). Finally, the percentage of MSBHs that form from the merger of a BH and a star is non-negligible at low metallicity (16 and 14 per cent at 0.1 $Z_\odot$ and 0.01 $Z_\odot$, respectively) and is very large at high metallicity (73 per cent at $Z_\odot$). As for the LBHs, in the vast majority of cases the BH and the star were already members of a binary before merging, and most of these BH-star binaries were not PBs. We recall that the mass of the product of a merger between two stars or a star and a BH is likely overestimated in our simulations, because no mass loss is assumed during the encounter. In the case of a merger between two stars, mass loss by stellar winds is accounted for, after the merger.

The vast majority of MSBHs that power RLO systems form from single stars at low metallicity (72 and 91 per cent at 0.1 $Z_\odot$ and 0.01 $Z_\odot$, respectively). This implies that dynamical exchanges are very important for RLO systems powered by MSBHs (as we will discuss in the next sections). A very small fraction of MSBHs that power RLO systems form from stars in PBs (only one system through all our simulations).

At low metallicity (0.1, 0.01 $Z_\odot$), the number of MSBHs that power RLO systems and form from the merger of two stars is negligible. In contrast, 33 per cent of MSBHs that power RLO systems form from the merger of two stars at $Z = Z_\odot$.

At $Z = 0.01$ $Z_\odot$ the percentage of MSBHs that power RLO systems and form from the merger of a star and a BH is negligible, while 22 per cent and 67 per cent of MSBHs powering RLO systems originate from the merger of a BH and a star at 0.1 $Z_\odot$ and $Z_\odot$, respectively. On the other hand, the absolute number of MSBHs that power RLO systems and originate from the merger of a BH and a star is low.

3.2. *The importance of exchanges*

The best way to quantify the impact of SC dynamics on the formation of RLO systems is to distinguish between primordial binaries (PBs, i.e. binaries that were already in the initial conditions) and binaries that formed through a dynamical exchange (EBs, i.e. binaries in which at least one of the two members entered the binary after a dynamical exchange). In our simulations (see Table 4), about 44 per cent of RLO binaries are EBs (corresponding to 107 systems), while the remaining 56 per cent are PBs (corresponding to 137 systems).

Fig. 1 compares the behavior of PBs that undergo RLO (hereafter RLO-PBs, blue open circles) with that of EBs that undergo RLO (hereafter RLO-EBs, red filled circles). RLO-EBs and RLO-PBs define two different groups: the former host typically more massive BHs than the latter, and tend to start the RLO phase later. The fact that RLO-EBs host more massive BHs is explained by the properties of exchanges: the probability for an exchange to occur is higher if the mass of the single object is higher than the mass of one of the former members of the binary (Hills 1989; Hills 1992).

The fact that PBs tend to start the RLO phase at earlier times is an indication that RLO in these systems is mainly driven by stellar evolution rather than by dynamics. The majority of RLO-PBs start the accretion episode immediately after the formation of the first BH (3-7 Myr), when the companion star evolves towards the terminal-age MS (TAMS) and its radius increases rapidly, filling the Roche lobe (RL). In contrast, more time is needed for an EB to enter the RLO. In particular, most EBs form during the core collapse (which starts at ~ 3 Myr and during which the maximum core density is reached, see Mapelli & Bressan 2013) and keep hardening (i.e. reducing their semi-major axis as a consequence of three-body encounters) for the next Myrs.

In Fig. 1, RLO systems from all simulated SCs are shown, without distinguishing between different metallicities. In Table 4, we consider different metallicities separately. There is an excess of RLO-PBs at low metallicity. The most likely explanation is that stellar radii are smaller at low metallicity, allowing a larger number of PBs to avoid merger before the formation of the first BH and to start RLO (see Linden et al. 2010).

Fig. 2 shows the main properties of RLO-PBs and RLO-EBs at different metallicities. EBs tend to enter a RLO phase later than PBs, regardless of metallicity. Furthermore, RLO-EBs tend to host more massive BHs than RLO-PBs. On the other hand, the maximum mass of the BHs powering the RLO systems strongly depends on metallicity: at $Z = 1$, 0.1 and 0.01 $Z_\odot$, the most massive BHs in RLO-EBs (RLO-PBs) have a mass ~ 38, 103 and 84 $M_\odot$ (~ 15, 20 and 48 $M_\odot$), respectively. The maximum mass of BHs in RLO-EBs at $Z = 1$ and 0.1 $Z_\odot$ is higher than the maximum BH mass that can be achieved through single-star evolution for these metallicities. Such high masses are the effect of BH-star mergers (see Section 3.1).

From Table 4 we can see that metal-poor SCs ($Z = 0.01 - 0.1$ $Z_\odot$) host a significant percentage (22–24 per cent) of RLO binaries powered by MSBHs (hereafter RLO-MSBHs). Solar-metallicity SCs host a small fraction (4 per cent) of RLO-MSBHs, which were born from star-star and BH-star merger. We emphasize that all RLO-MSBHs but one are EBs. The importance of RLO-MSBHs will be further investigated in the next Section.

Table 4
Summary of the properties of simulated RLO systems.

Z ($Z_\odot$)	RLO	RLO-PBs	RLO-EBs	RLO-MSBHs	RLO-LBHs
0.01	89	57	32	21	68
0.1	82	45	37	18	64
1.0	73	35	38	3	70
All[a]	244	137	107	42	202

Note. — *Notes.* Z (column 1): metallicity of the SC; RLO (column 2): number of all simulated RLO systems; RLO-PBs (column 3): number of PBs that undergo RLO; RLO-EBs (column 4): number of EBs that undergo RLO; RLO-MSBHs (column 5): number of RLO systems powered by MSBHs; RLO-LBHs (column 6): number of RLO systems powered by BHs with mass<25 $M_\odot$ for different metallicities and in total.
[a]'All' refers to the statistics of all runs without distinguishing between different metallicities.

Another difference between RLO-EBs and RLO-PBs is the mass range of donor stars: RLO-EBs have less massive donor stars than RLO-PBs. This is due to the fact that EBs start the RLO phase later than PBs, when the turn-off (TO) mass is smaller. The maximum mass of donor stars in RLO-PBs is clearly affected by stellar winds: the maximum mass of a donor star is $\gtrsim 100$ $M_\odot$ at $Z = 0.01$ $Z_\odot$, where stellar winds are negligible, while it is $\lesssim 60$ $M_\odot$ at $Z = Z_\odot$. Finally, the orbital periods tend to be longer in RLO-EBs than in RLO-PBs, especially at very low metallicity ($Z = 0.01$ $Z_\odot$). Thus, the former tend to start the RLO phase only when the companion star evolves off the MS. RLO systems with longer period host either more massive BHs (with large RL) or post-MS donor stars (with large radius).

3.3. *MSBHs versus light BHs*

As we mentioned in the previous section, RLO systems powered by MSBHs (hereafter RLO-MSBHs) are basically a sub-group of RLO-EBs, since all RLO-MSBHs but one are EBs (see Figures 1, 2 and 3). This confirms one of the most important results of M13, i.e. that dynamics is essential to drive the formation of RLO-MSBHs. As already shown by Linden et al. (2010), isolated binaries can hardly evolve into RLO-MSBHs (even if they have a sufficiently small initial semi-major axis), because mass-transfer and common-envelope phases (before the formation of the first BH) cause either the two stars to merge or the first BH to be much lighter than in case of a single-star progenitor. Thus, RLO-MSBHs are expected to be very rare among isolated field binaries. In contrast, in a dense SC, single MSBHs can acquire companions through dynamical exchanges and power RLO systems.

Most simulated MSBHs are born from direct collapse of metal-poor stars (~ 79 per cent of all MSBHs in RLO systems), but a fraction of MSBHs can form and/or grow in mass through mergers with other stars. This explains why there is a non-zero fraction of MSBHs even at solar metallicity. In particular, 9 MSBHs that power RLO systems (corresponding to ~ 21 per cent of all RLO-MSBHs) come from the merger of either two stars or a BH and a star (Table 3).

In our simulations, 24 and 22 per cent of all BHs that power RLO systems are MSBHs at $Z = 0.01$ and 0.1 $Z_\odot$, respectively (see Table 4). Since MSBHs are only ~ 18

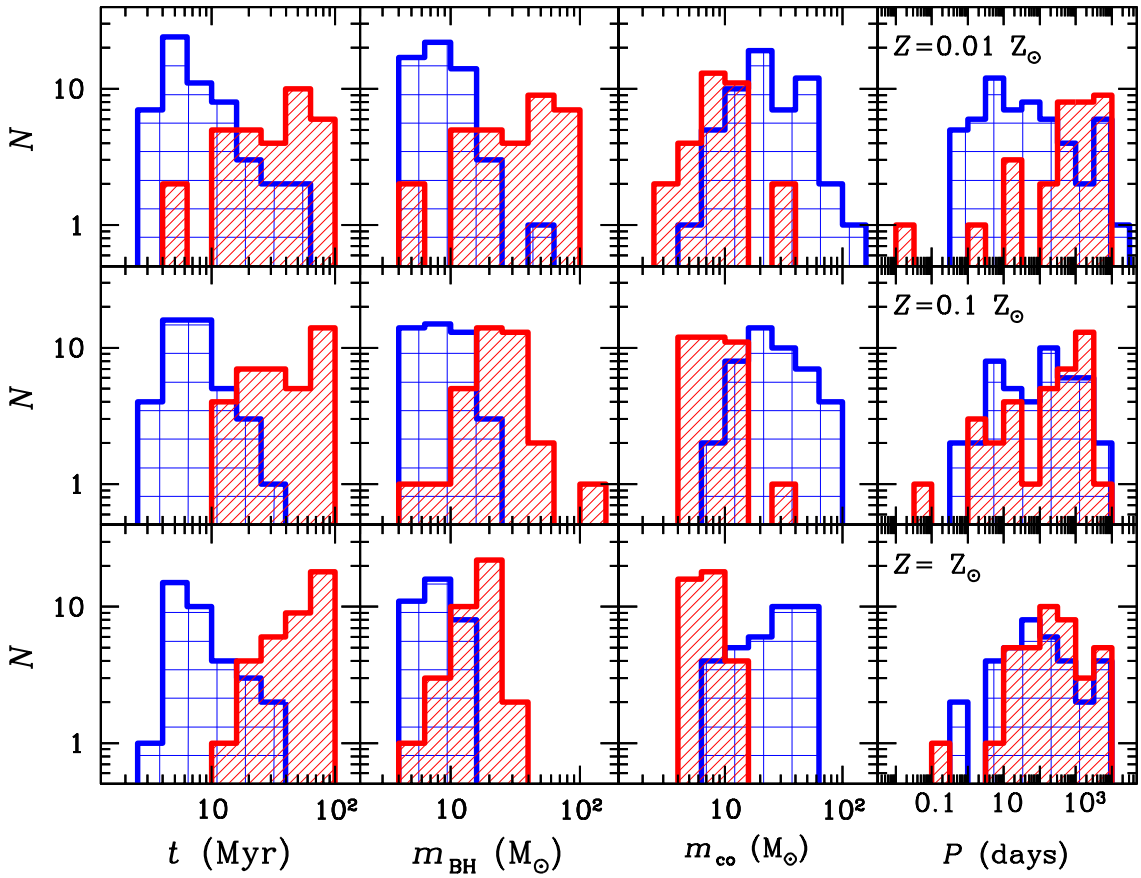

Figure 2. From left to right: time t when the RLO phase starts ($t = 0$ is the beginning of the simulation), mass of the BH in RLO systems ($m_{\rm BH}$), mass of the donor star in RLO systems ($m_{\rm co}$), orbital period (P) at the beginning of the RLO phase. From top to bottom: $Z = 0.01$ Z$_\odot$, 0.1 Z$_\odot$ and 1 Z$_\odot$. Red hatched histogram (blue cross-hatched histogram) refers to RLO-EBs (RLO-PBs).

per cent of all BHs at $Z = 0.01-0.1$ Z$_\odot$ (see Tables 2 and 3), this implies that MSBHs have a higher probability of powering RLO systems than low-mass BHs. At $Z = $ Z$_\odot$ about 4 per cent of all BHs that power RLO systems are MSBHs born from mergers.

Fig. 4 compares the main properties of RLO-MSBHs with those of RLO systems powered by 'light' (< 25 M$_\odot$) BHs (hereafter RLO-LBHs). RLO-MSBHs behave in the same way as other RLO-EBs: they start the RLO phase generally later than light BHs and have smaller donor stars.

3.4. *Properties of the donor stars*

Our $N-$body simulations contain information about the mass, radius (R), luminosity (L) and effective temperature ($T_{\rm eff}$) of the stars, and account for their dependence on time and metallicity. Thus, we can investigate the observational signatures of the donor stars at the time they fill their RL.

Fig. 5 shows the Hertzsprung-Russell (HR) diagram of the donor stars when they fill the RL for the first time. It is apparent that a large portion of donor stars are in the MS or in the red-giant branch. Table 5 summarizes the types of donor stars at the first RL approach. A large percentage of donor stars ($\sim 33-50$ per cent, depending on the metallicity) are either in the MS or in the Hertzsprung gap (i.e. they just left the MS). A similar percentage ($28-40$ per cent) is either in the red-giant or in the red-supergiant branch. A significant fraction ($15-21$ per cent) is composed of hypergiant stars. Blue loop and WR stars are much less frequent. Finally, two donor stars are in the LBV phase, corresponding to ~ 0.8 per cent of all donor stars.

We notice that MS stars are the most important group of donor stars at low metallicity ($Z = 0.01-0.1$ Z$_\odot$) while red-giant stars are more frequent at high metallicity ($Z = $ Z$_\odot$). The main reason is that the stellar radii are smaller at low metallicity, allowing a larger number of PBs to avoid merger before the formation of the first BH and to start RLO when the donor is still a MS, or immediately after (see also the discussion in Linden et al. 2010). This is supported by the fact that the number of RLO-PBs is ~ 40 per cent higher at $Z = 0.01$ Z$_\odot$ than at $Z = 1$ Z$_\odot$ (see Section 3.2 and Table 4).

Finally, we notice that a large portion of binaries that undergo RLO will merge at the end of the RLO phase or within the next 2 Myrs (76, 87 and 79 per cent at $Z = 0.01$, 0.1 and 1 Z$_\odot$, respectively).

3.5. *The contribution of the accretion disk*

In the previous Section, we analyzed the observational signatures of the simulated donor stars. On the other hand, the contribution of the irradiated accretion disk might significantly affect the optical luminosity and colors of the observed counterparts (e.g. Copperwheat et al. 2005; Copperwheat et al. 2007; Mucciarelli et al. 2007;

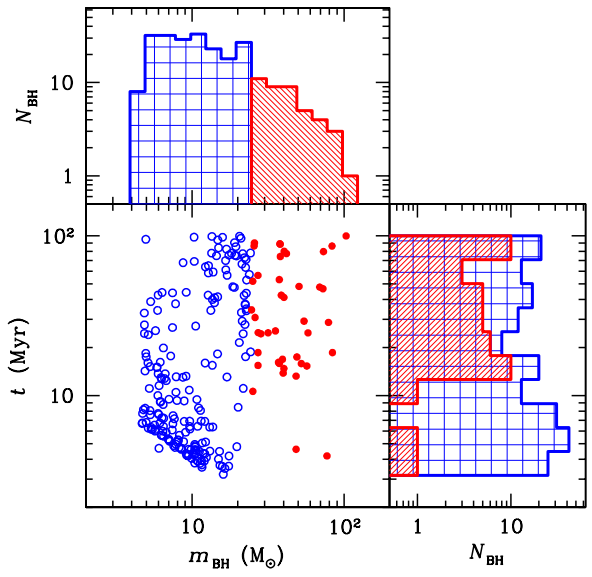

Figure 3. Main window: mass of the BHs that power simulated RLO systems versus the time when the RLO phase starts. Red filled circles: RLO-MSBHs (i.e. RLO systems powered by MSBHs); blue open circles: RLO-LBHs (i.e. RLO systems powered by BHs with mass < 25 $M_\odot$). The marginal histograms show the distribution of the masses of BHs that power RLO systems and the distribution of the times when the RLO phase starts ($t = 0$ is the beginning of the simulation). In both marginal histograms, the red hatched histogram (blue cross-hatched histogram) refers to RLO-MSBHs (RLO-LBHs). In this plot, as in Fig. 1, all the simulated SCs are shown, and we do not distinguish between different metallicities.

Table 5
Percentage of donor stars divided by type[a].

Z ($Z_\odot$)	MS & HG (%)	Hy (%)	RG (%)	BL (%)	WR (%)	LBV (%)
0.01	50	15	31	1	2	1
0.1	45	21	28	4	1	1
1	33	19	40	5	3	0
All[b]	43	19	33	3	2	< 1

Note. — *Notes.* [a]Percentages for each type of donor stars and for different metallicity. MS: main-sequence stars, HG: Hertzsprung gap stars (generally stars that just left the MS), Hy: hypergiant stars, RG: red-giant stars and red-supergiant stars, BL: blue loop stars, WR: Wolf-Rayet stars, LBV: luminous blue variable stars.
[b]'All' refers to the statistics of all runs without distinguishing between different metallicities.

Patruno & Zampieri 2008; Patruno & Zampieri 2010; Madhusudhan et al. 2008; Grisé et al. 2012).

Thus, we use the code described in Patruno & Zampieri (2008, 2010) to model the optical emission associated with the simulated RLO binaries. The code accounts for both the emission of the donor star and the emission due to X-ray reprocessing of the accretion disk and of the donor star. A Shakura-Sunyaev disk is assumed. If the accretion rate reaches the Eddington limit (for a standard accretion efficiency of ~ 0.1), the luminosity is limited at Eddington and the excess mass is assumed to be expelled from the system. A simplified description of radiative transfer for the interaction of the X-rays with the disk and donor surfaces is adopted (an X-ray illuminated plane-parallel atmosphere in radiative equilibrium; e.g. Copperwheat et al. 2005). The model does not include a Comptonization of disk emission in a corona. We assume inclination $i = 0$ (face-on disk) and albedo $= 0.9$. The fraction of X-ray flux thermalized in the outer irradiated disk is typically in the range $0.004 - 0.008$.

The $N-$body simulations provide information about (i) the radius, mass, optical luminosity, effective temperature and age of the donor star when it fills its RL; (ii) the mass of the BH; (iii) the orbital properties of the binary when it starts the RLO phase (orbital period). These properties of the simulated RLO systems are fed to the Patruno & Zampieri (2008) code, to model the optical luminosity and colors.

The results indicate the overall importance of disk irradiation: the flux from the disk ($F_{\rm disk}$) ranges from ~ 0.1 to $\sim 10^4$ times the flux from the donor star ($F_{\rm co}$). The highest values of $F_{\rm disk}/F_{\rm co}$ are associated with the most massive MSBH systems ($Z = 0.01$ $Z_\odot$), which have the most extended accretion disks and the faintest donor stars (red giant stars with $M \sim 5 - 10$ $M_\odot$).

Figures 6 and 7 show the $V-$band magnitude and the $B - V$ color (Johnson filters) of the simulated RLO systems, assuming a distance of 5 Mpc. RLO-EBs and RLO-PBs are compared in Fig. 6, while RLO-MSBHs and RLO-LBHs are compared in Fig. 7.

The $B - V$ color shows interesting features. The bluer RLO systems $[-0.35 < (B-V) < 0]$ span a large range of magnitudes, from $V \sim 20$ to $V \sim 27$. Instead, the redder RLO systems define a narrower sequence in Figures 6 and 7, which can be approximated as $V \approx 24.3 - 1.6\,(B-V)$ with a conspicuous scatter, larger at bluer colors[4].

This behavior is explained by the mass range of the donor stars. The most massive young donor stars are generally associated with blue counterparts, while lower mass donor stars are found in both blue and red counterparts (depending on the relative importance of the disk). Thus, blue systems have a large scatter in V, since they can host both massive (> 30 $M_\odot$), very bright donor stars and lower-mass (5–20 $M_\odot$), less luminous donor stars (see Fig. 8). In contrast, red systems are generally disk dominated and host only lower-mass (5–20 $M_\odot$) older stars, mostly red giant stars.

Also, we notice that the sequence defined by $V \approx 24.3 - 1.6\,(B - V)$ is mainly populated by RLO-EBs (see Fig. 6), whose donor stars are predominantly older and less-massive than those of RLO-PBs (see Fig. 2). In contrast, RLO-PBs are mostly associated with the bluer counterparts. In both cases, there are some remarkable exceptions (i.e. very blue RLO-EBs and very red RLO-PBs).

Even in the CMD, RLO-MSBHs behave as a sub-group of RLO-EBs, since the former populate the same sequence as the latter. On the other hand, RLO-MSBHs represent the high-luminosity tail of RLO-EBs, since they populate mainly the upper envelope of the sequence. RLO-MSBHs span a narrower range of V magnitudes ($19.5 < V < 25.5$) than RLO-LBHs, and ~ 80 per cent of RLO-MSBHs have $22 < V < 24$. The counterparts of RLO-MSBHs are predominantly red, with a peak at $B - V \sim 0.3$.

The position of the counterparts in the CMD of Fig-

[4] $V \approx 24.3 - 1.6\,(B - V)$ comes from the least square fit of the simulated RLO-EBs, excluding the four outliers with $V < 20.5$.

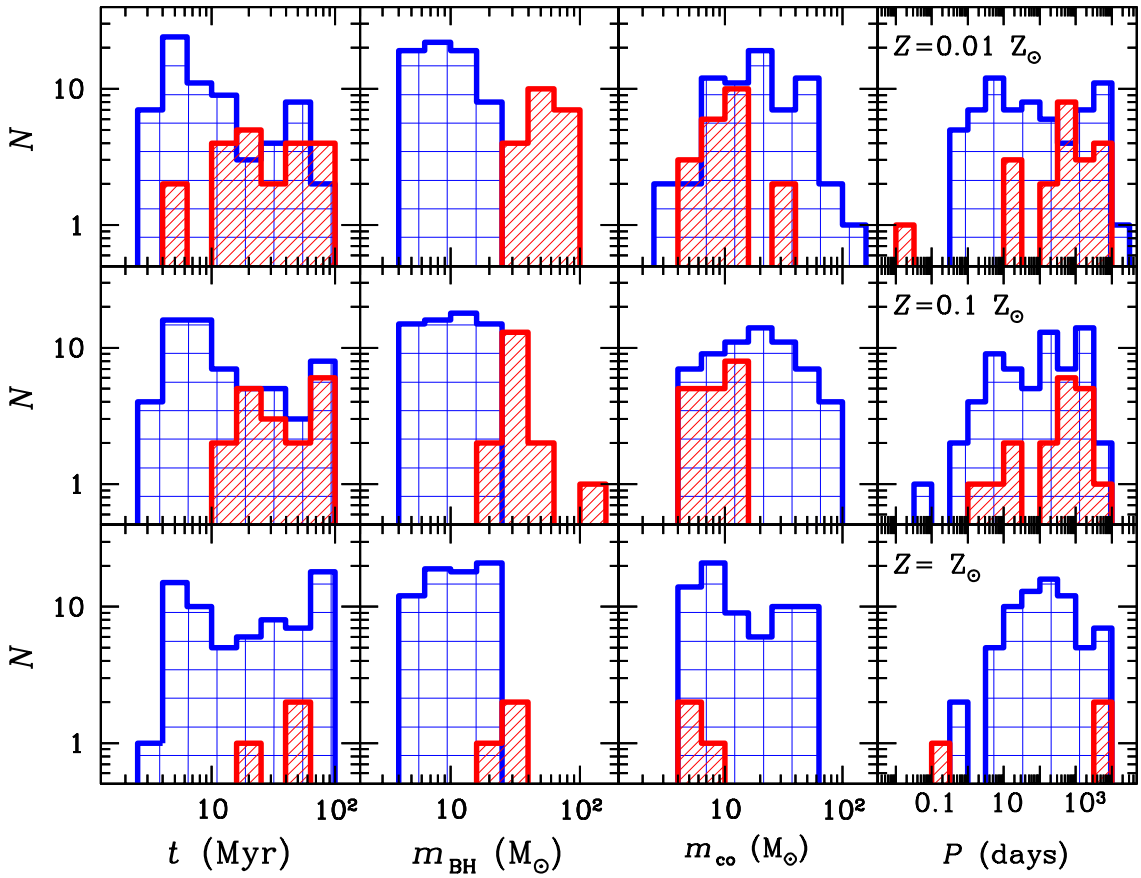

Figure 4. From left to right: time t when the RLO phase starts ($t = 0$ is the beginning of the simulation), mass of the BH in RLO systems ($m_{\rm BH}$), mass of the donor star in RLO systems ($m_{\rm co}$), orbital period at first RL approach (P). From top to bottom: $Z = 0.01$ $Z_\odot$, 0.1 $Z_\odot$ and 1 $Z_\odot$. Red hatched histograms and blue cross-hatched histograms refer to RLO-MSBHs and RLO-LBHs, respectively.

ures 6 and 7 can be understood as follows. The majority of the blue ($B-V < -0.1$) systems have MS companions, with masses from ~ 10 M$_\odot$ to several tens of M$_\odot$. Very massive companions (> 20 M$_\odot$) are sufficiently bright that their intrinsically blue emission dominates over that of the accretion disk. Lower mass companions ($10 - 20$ M$_\odot$) are weaker and the contribution of the disk is significant for them. They typically reside in tighter systems ($P < 5 - 10$ d). As a consequence, their disk is not very extended and the combined disk plus donor emission appears as blue as that of higher mass systems.

On the other hand, donors in the $10-20$ M$_\odot$ range can also reside in systems with intermediate colors ($-0.1 < B - V < 0.2$), if they are slightly more evolved and at larger orbital separations ($P > 5 - 10$ d). The disk is then more extended and its optical spectrum appears redder. Markedly red counterparts ($B - V > 0.2$) are produced by large-separation systems with very extended disks, the outer parts of which are strongly irradiated and emit significantly in the near-infrared band. For the largest systems ($P > 100$ d) the flux of the $10 - 20$ M$_\odot$ evolved companion may overcome that of the disk. These systems host most MSBHs, since they typically form at later times (when > 20 M$_\odot$ stars have already evolved) and from dynamical interactions.

Finally, the eight systems with $V < 20$ are outliers: four of them are systems that are undergoing a merger, while in the other four systems the donor star evolves very rapidly and the $N-$body outputs are not frequent enough to capture the fast changes of the properties of the donor star (i.e. there is a mismatch between the last time-step in which the radius was calculated and the time when the RLO phase starts).

4. DISCUSSION

4.1. *Ultraluminous X-ray sources and simulated RLO binaries*

Figures 6 and 7 show that the simulated RLO systems describe a well-defined pattern in the CMD. In particular, RLO-EBs and RLO-PBs behave in two different ways, since the former are generally redder than the latter. In the CMD, RLO-MSBHs follow the same trend as RLO-EBs, since all RLO-MSBHs but one formed from dynamical exchange. On the other hand, RLO-MSBHs represent the high-luminosity envelope of RLO-EBs in the CMD.

These results provide important insights to understand the observations of bright X-ray binaries in young SCs. Comparing the simulations with a complete set of data is beyond the aims of this paper. In this section, we will focus on a specific class of X-ray binaries, the ULXs. We chose the ULXs because they are mostly associated with star forming regions and/or young SCs (e.g. Zezas et al. 2002; Kaaret et al. 2004; Berghea 2009; Mapelli et al. 2010; Poutanen et al. 2013; Berghea et al. 2013), because they

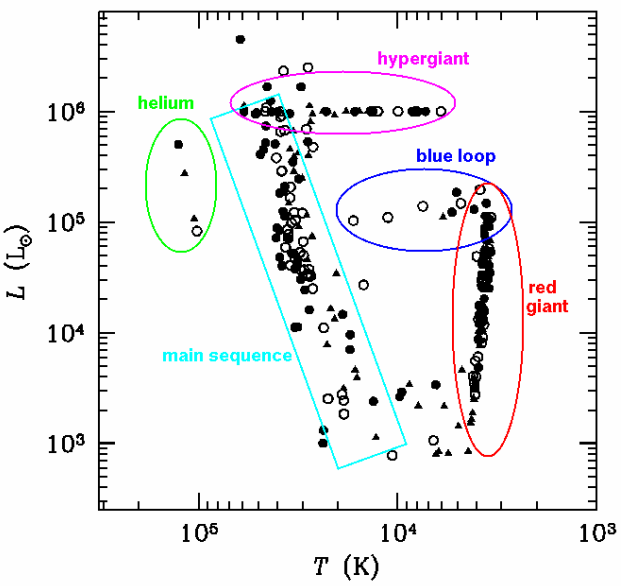

Figure 5. HR diagram of the simulated donor stars when they fill the RL. Filled circles: $Z = 0.01$ Z$_\odot$; open circles: $Z = 0.1$ Z$_\odot$; filled triangles: $Z =$ Z$_\odot$. The colored ellipses and boxes approximately indicate the most common types of donor stars. In particular: MS (cyan box), red-giant and supergiant stars (red ellipse), blue loop stars (blue ellipse), hypergiant stars (magenta ellipse) and naked-core helium stars (green ellipse).

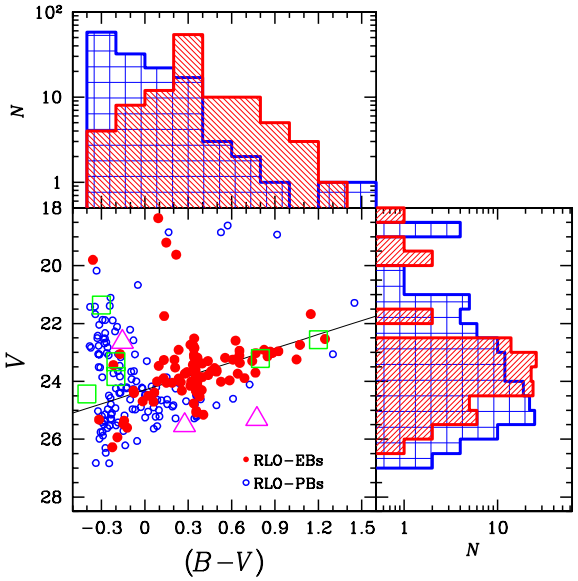

Figure 6. Main window: CMD (in the Johnson B and V filters) of the simulated RLO systems. The magnitudes take into account both the flux from the donor star and the flux from the irradiated disk (see the main text for details). Red filled circles: RLO-EBs (i.e. EBs undergoing RLO); blue open circles: RLO-PBs (i.e. PBs undergoing RLO). In the marginal histograms, red diagonal-hatched histogram: RLO-EBs; blue cross-hatched histogram: RLO-PBs. Green open squares: counterparts of six ULXs from Gladstone et al. (2013, M81 X-6, Ho IX X-1, NGC 1313 X-1, NGC 1313 X-2, IC 342 X-1 and NGC 3034 ULX5) in the F435W and F555W *HST* filters. Magenta open triangles: counterparts of three ULXs from Gladstone et al. (2013, NGC 2403 X-1, M83 XMM1 and NGC 5204 X-1) in the F435W and F606W *HST* filters (the F606W filter was adapted to the F555W filter as discussed in Appendix A). Both the simulated and the observed magnitudes are apparent magnitudes (in Vega mag) obtained assuming that all sources are at 5 Mpc distance. The solid line corresponds to the $V \approx 24.3 - 1.6\,(B-V)$ sequence of RLO-EBs (see the text for details).

seem to anti-correlate with the local metallicity (e.g. Pakull & Mirioni 2002; Zampieri et al. 2004; Soria et al. 2005; Swartz, Tennant & Soria 2009; Mapelli et al. 2009; Mapelli et al. 2010; Mapelli et al. 2011a; Kaaret & Feng 2013; Prestwich et al. 2013) and because they have an estimated luminosity (assuming isotropy) higher than the Eddington luminosity of a 10 M$_\odot$ BH. For the high luminosity and for the anti-correlation with metallicity, Mapelli et al. (2009) proposed that (a fraction of) ULXs are associated with MSBHs (see also Zampieri & Roberts 2009; Mapelli et al. 2010; Mapelli et al. 2011a).

Unfortunately, identified counterparts are available in the literature only for a limited number of ULXs. The most recent and homogeneous sample of optical ULX counterparts has been reported by Gladstone et al. (2013, hereafter G13). Among the 22 ULXs studied in G13 that have *Chandra* observations, and that have at least one detected possible counterpart from *Hubble Space Telescope* (*HST*) data, we selected nine sources (see Table 6), based on the criteria described in Appendix A.

Five of the nine considered sources (Ho IX X-1, NGC 1313 X-2, IC 342 X-1, NGC 5204 X-1 and NGC 3034 ULX5) have multiple possible counterparts in the *Chandra* error box. In Table 6, and in Figures 6 and 7, we report only the counterparts that were selected based on the criteria described in Appendix A. In Figures 6 and 7, we show apparent magnitudes obtained positioning both the observed counterparts and the simulated ones at a distance of 5 Mpc.

From Figures 6 and 7, it is apparent that the observed counterparts populate the same regions in the CMD as the simulated ones. In Table 7, we list all the simulated systems that have Eddington luminosity $L_{\rm Edd} \geq 0.1\,L_{\rm X,\,max}$ (where $L_{\rm X,\,max}$ is the maximum observed X-ray luminosity) and that differ from the observed counterparts by $|\Delta_{\rm V}| < 0.5$ (where $\Delta_{\rm V}$ is the difference between simulated and observed V magnitude) and by $|\Delta_{\rm B-V}| < 0.2$ (where $\Delta_{\rm B-V}$ is the difference between simulated and observed $B-V$ color). The requirement that $L_{\rm Edd} \geq 0.1\,L_{\rm X,\,max}$ is necessary because our models have been calculated under the assumption of sub-Eddington accretion: a strongly super-Eddington accretion and/or the presence of beaming would affect the optical counterpart significantly and cannot be accounted for by our current models. The tolerance ranges in V and $B-V$ account for the fact that some observed ULX counterparts are known to vary significantly (e.g. NGC 1313 X-2, Mucciarelli et al. 2007; Grisé et al. 2008; Liu et al. 2009; Ho IX X-1, Grisé et al. 2011).

We do not find any simulated systems that satisfy the aforementioned requirements in the case of both M83 XMM1 and NGC 3034 ULX5. M83 XMM1 is one of the three sources for which the V magnitude was derived from the F606W filter, likely introducing a larger uncertainty. In Table 7, we report the simulated system which is closer to the observed counterpart of M83 XMM1: it has $\Delta_{\rm B-V} = -0.28$ and $\Delta_{\rm V} = -0.48$.

In the case of NGC 3034 ULX5, all the simulated systems that match the criteria on optical magnitude and

Table 6
Selected ULX counterparts from G13.

Name	ID	DM	F435W	F555W	F606W	V	$(B-V)$	Z ($Z_\odot$)	P (days)	$L_{X,\,max}$ (10^{39} erg s^{-1})	Ref.
M81 X-6	1	31.13	23.7	24.0	23.8	21.36	-0.3	0.40 – 0.22	–	6.7	(1)
Ho IX X-1	1	27.67	22.3	22.5	NO	23.32	-0.2	0.38	–	28	(2)
NGC 1313 X-1	1	28.06	23.6	24.0	23.7	24.43	-0.4	0.10	–	15	(3)
NGC 1313 X-2	1	28.06	23.2	23.4	NO	23.83	-0.2	0.10	6, 12	8.1	(3)
IC 342 X-1	1	27.58	23.1	22.3	21.9	23.21	0.8	0.37 – 0.11	–	13.3	(2)
NGC 2403 X-1	1	27.70	25.0	NO	24.5	25.52	0.275	0.29 – 0.18	–	3.6	(1)
M83 XMM1	1	28.41	26.0	NO	25.0	25.31	0.775	0.42 – 0.32	–	2.8	(1)
NGC 5204 X-1	1	28.38	22.37	NO	22.3	22.64	-0.155	–	–	8.7	(2)
NGC 3034 ULX5	1	27.73	23.0	21.8	NO	22.56	1.2	–	62	79	(4)

Note. — *Notes.* Column 1: ULX name; column 2: identification number of the counterpart from Table 4 of G13; column 3: distance modulus (DM); column 4: magnitude in F435W filter (from Table 4 of G13); column 5: magnitude in F555W filter (from Table 4 of G13); column 6: magnitude in F606W filter (from Table 4 of G13); column 7: V magnitude obtained positioning the source at 5 Mpc. V is obtained from F555W or, when F555W is not available, from F606W (converted into F555W as described in the text). V is shown in Figures 6 and 7. Column 8: $(B-V)$ color. The B magnitude is obtained from the F435W filter, positioning the source at 5 Mpc. V is the same as tabulated in column 7. $(B-V)$ is shown in Figures 6 and 7. Column 9: Metallicity Z of the host galaxy. The integrated metallicity of the galaxy is given for Ho IX and NGC 1313, while the metallicity range indicated for the other galaxies corresponds to the metallicity between 0.4 and 1 R_{25} (R_{25} being the isophotal radius, de Vaucouleurs et al. 1991). Metallicities were derived from spectroscopy of HII regions as described in Mapelli et al. (2010). Metallicity values for M81, NGC 1313, IC 342, NGC 2403 and M83 come from Mapelli et al. (2010, and references therein), while the metallicity of Ho IX comes from Makarova et al. (2002). For NGC 5204 and NGC 3034 no metallicity estimates are available that can be directly compared with those of the other galaxies. Column 10: Orbital period (P) as derived from observations. An estimate of the period is available only for NGC 3034 ULX5 and for NGC 1313 X-2. In the case of NGC 1313 X-2, P might be either 6 d or 12 d (Liu et al. 2009), depending on the relative importance of the variations induced by X-ray irradiation and ellipsoidal modulation of the donor. Column 11: $L_{X,\,max}$ is the maximum observed X-ray luminosity. Column 12: references for $L_{X,\,max}$: (1) Winter et al. (2006), (2) Pintore et al. (2014), (3) Pintore & Zampieri (2012), (4) Feng & Kaaret (2010).
In columns 5–6: 'NO' stands for 'the source was not observed with this filter' (see G13 for details). The magnitudes provided in this table are Vega magnitudes and are corrected for Galactic extinction but not for intrinsic extinction.

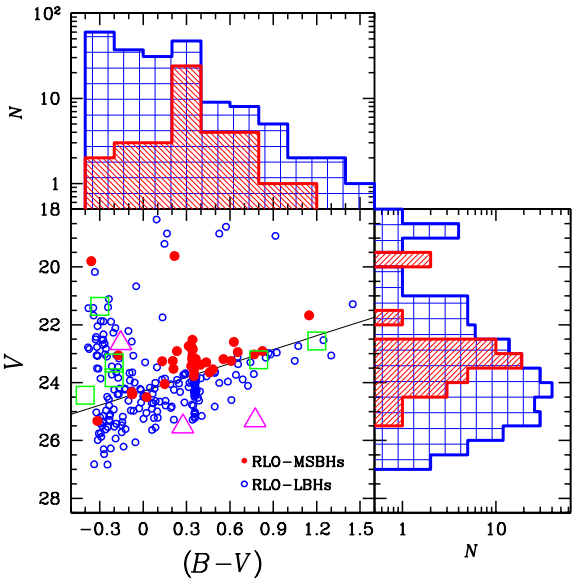

Figure 7. The same as Fig. 6, but for RLO-MSBHs and RLO-LBHs. In particular, in the main window, red filled circles: RLO-MSBHs; blue open circles: RLO-LBHs. In the marginal histograms, red diagonal-hatched histogram: RLO-MSBHs; blue cross-hatched histogram: RLO-LBHs.

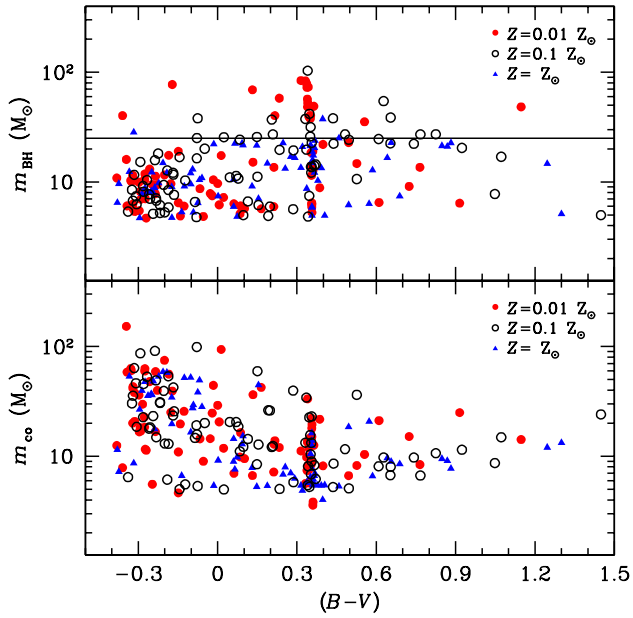

Figure 8. Top (bottom) panel: mass of the BH (donor star) of the simulated RLO systems versus the $B-V$ color. In both panels, filled red circles: systems with $Z = 0.01$ $Z_\odot$, open black circles: systems with $Z = 0.1$ $Z_\odot$, filled blue triangles: systems with $Z = 1$ $Z_\odot$. The horizontal line in the top panel marks the separation between light BHs and MSBHs (i.e. the threshold mass $m_{BH} = 25$ $M_\odot$). The simulated magnitudes are apparent magnitudes (in Vega mag) obtained assuming that all sources are at 5 Mpc distance.

color have $L_{Edd} \ll 0.1\,L_{X,\,max}$. In Table 7, we report the simulated system which is closer to the observed counterpart according to Δ_{B-V} and Δ_V, but has $L_{Edd} \sim 0.02\,L_{X,\,max}$. NGC 3034 ULX5 (also known as M82 X-1) is an outlier of our sample, under many respects. First, the intrinsic extinction is expected to be very high, but cannot be reliably quantified (G13). Second, the best-matching simulated system has much longer orbital period (5000 d) than the observed one (62 d, Kaaret et al. 2006). Third, the maximum observed X-ray luminosity is by far the highest in the sample (Feng & Kaaret 2010). This source likely belongs to a completely different class (an intermediate-mass BH has been required to explain some of its properties, e.g. Kaaret et al. 2001; Patruno et al. 2006; Casella et al. 2008; Feng & Kaaret 2010).

In the other cases, we come to some remarkable results. The counterparts of M81 X-6 and NGC 1313 X-1 are matched only by simulated RLO-PBs, the counterparts of NGC 1313 X-2, NGC 2403 X-1 and NGC 5204 X-1 are matched by both simulated RLO-PBs and simulated RLO-EBs, while the counterparts of Ho IX X-1 and IC 342 X-1 are matched only by simulated RLO-EBs. Considering the three observed counterparts that

Table 7
Simulated systems that best match the selected ULX counterparts from G13

Name	$\Delta_{\rm V}$	$\Delta_{\rm B-V}$	P (days)	$m_{\rm co}$ ($M_\odot$)	$m_{\rm BH}$ ($M_\odot$)	Z ($Z_\odot$)	Binary type	$L_{\rm Edd}$ (10^{39} erg s^{-1})
M81 X-6	0.05	-0.05	8.13	152.5	16.0	0.01	PB	2.09
M81 X-6	-0.26	0.06	257	91.2	15.8	0.1	PB	2.05
M81 X-6	0.03	0.06	80.8	48.2	7.9	1.0	PB	1.03
M81 X-6	0.06	-0.08	0.420	11.5	6.5	1.0	PB	0.84
M81 X-6	0.31	-0.04	8.51	58.4	6.0	0.01	PB	0.79
Ho IX X-1	-0.27	0.03	10.3	39.3	77.3	0.01	EB	10.05
NGC 1313 X-1	0.06	0.15	6.98	36.2	12.3	1.0	PB	1.59
NGC 1313 X-1	-0.19	0.20	25.7	74.9	11.6	0.01	PB	1.51
NGC 1313 X-2	0.49	0.12	11.0	15.8	25.1	0.1	EB	3.26
NGC 1313 X-2	-0.17	0.11	83.2	27.5	13.1	1.0	PB	1.70
NGC 1313 X-2	0.41	-0.0009	25.7	74.9	11.6	0.01	PB	1.51
NGC 1313 X-2	0.16	0.14	65.8	28.2	10.9	1.0	PB	1.41
NGC 1313 X-2	0.42	0.18	69.4	44.3	10.5	0.01	PB	1.36
NGC 1313 X-2	0.37	0.07	42.1	52.0	9.1	1.0	PB	1.19
NGC 1313 X-2	-0.37	0.03	70.2	34.4	9.1	1.0	PB	1.18
NGC 1313 X-2	-0.18	0.01	155	53.6	8.5	0.1	PB	1.10
NGC 1313 X-2	0.37	0.04	46.8	25.7	7.6	0.1	PB	0.99
NGC 1313 X-2	0.38	0.18	375	24.7	7.5	0.01	PB	0.97
NGC 1313 X-2	-0.31	-0.11	12.2	46.3	7.4	0.1	PB	0.96
NGC 1313 X-2	-0.33	-0.12	12.8	35.6	6.7	0.1	PB	0.88
NGC 1313 X-2	-0.19	0.12	408	38.3	6.5	1.0	PB	0.84
IC 342 X-1	-0.27	-0.15	1435	8.0	38.6	0.1	EB	5.02
IC 342 X-1	-0.30	0.03	1495	10.7	27.2	0.1	EB	3.54
IC 342 X-1	-0.19	-0.03	1094	6.7	27.1	0.1	EB	3.53
IC 342 X-1	0.04	-0.19	194.5	8.1	24.6	0.1	EB	3.20
IC 342 X-1	0.15	-0.14	857	8.9	22.7	1.0	EB	2.96
IC 342 X-1	-0.19	0.08	3713	7.7	22.7	1.0	EB	2.95
IC 342 X-1	-0.10	-0.15	140	6.7	22.5	0.1	EB	2.92
IC 342 X-1	0.08	-0.06	3007	9.7	22.3	0.1	EB	2.89
IC 342 X-1	-0.08	0.05	2976	9.5	21.3	1.0	EB	2.78
IC 342 X-1	-0.24	0.07	313	9.1	21.1	1.0	EB	2.74
IC 342 X-1	-0.25	0.12	1655	11.5	20.4	0.1	EB	2.66
IC 342 X-1	0.49	-0.04	6533	8.4	13.6	0.01	EB	1.77
NGC 2403 X-1	-0.49	0.08	3916	15.1	6.3	0.01	EB	0.82
NGC 2403 X-1	-0.48	0.08	4221	15.0	6.2	0.01	PB	0.81
NGC 2403 X-1	-0.24	-0.06	60.5	7.2	6.0	0.01	PB	0.78
NGC 2403 X-1	-0.44	0.08	8113	9.1	5.9	0.01	EB	0.77
NGC 2403 X-1	-0.44	0.08	2768	16.3	5.9	1.0	PB	0.77
NGC 2403 X-1	-0.44	0.08	7616	13.9	5.9	1.0	PB	0.76
NGC 2403 X-1	-0.30	-0.17	54.8	9.5	5.7	0.01	PB	0.75
NGC 2403 X-1	-0.34	0.08	6711	19.4	5.3	0.01	PB	0.69
NGC 2403 X-1	0.03	-0.19	35.4	9.9	5.1	0.01	PB	0.67
NGC 2403 X-1	-0.29	0.08	5227	12.5	5.0	1.0	PB	0.64
NGC 2403 X-1	-0.37	0.13	852	5.5	5.0	1.0	EB	0.64
NGC 2403 X-1	-0.24	0.07	354	8.1	4.8	0.1	PB	0.63
M83 XMM1	-0.48	-0.28	2007	18.5	6.2	1.0	PB	0.80
NGC 5204 X-1	0.42	-0.02	10.3	39.3	77.3	0.01	EB	10.05
NGC 5204 X-1	0.42	-0.03	170	56.0	17.5	0.01	PB	2.28
NGC 5204 X-1	-0.06	0.08	138	99.0	16.4	0.1	PB	2.14
NGC 5204 X-1	-0.36	-0.05	105	58.7	14.9	1.0	PB	1.94
NGC 5204 X-1	0.19	-0.10	61.1	47.9	13.1	0.01	PB	1.70
NGC 5204 X-1	-0.43	0.05	271	52.2	12.0	1.0	PB	1.56
NGC 5204 X-1	0.43	-0.17	0.445	20.0	11.5	0.01	PB	1.50
NGC 5204 X-1	-0.12	-0.12	166	59.7	10.6	0.01	PB	1.37
NGC 5204 X-1	0.43	0.09	402	49.4	10.5	1.0	PB	1.36
NGC 5204 X-1	0.01	-0.11	119	53.0	10.4	0.1	PB	1.35
NGC 5204 X-1	0.44	-0.16	8.55	38.1	10.4	0.01	PB	1.35
NGC 5204 X-1	-0.13	-0.17	7.70	63.0	10.3	0.01	PB	1.34
NGC 5204 X-1	-0.22	-0.17	9.33	60.3	10.1	0.01	PB	1.31
NGC 5204 X-1	-0.31	-0.12	33.4	47.7	8.8	1.0	PB	1.14
NGC 5204 X-1	0.46	-0.10	29.7	37.0	8.2	1.0	PB	1.07
NGC 5204 X-1	0.05	-0.13	98.5	45.5	8.1	0.1	PB	1.06
NGC 5204 X-1	0.38	-0.11	26.6	35.7	8.1	1.0	PB	1.05
NGC 5204 X-1	-0.11	-0.13	21.3	39.6	7.8	1.0	PB	1.02
NGC 3034 ULX5	-0.03	0.05	5054	12.0	14.7	1.0	EB	1.91

Note. — *Notes.* Column 1: ULX name; column 2: $\Delta_{\rm V} \equiv V_{\rm sim} - V_{\rm obs}$, i.e. difference between simulated and observed V magnitude; column 3: $\Delta_{\rm B-V} \equiv [(B_{\rm sim} - V_{\rm sim}) - (B_{\rm obs} - V_{\rm obs})]$, i.e. difference between simulated and observed $B-V$ color; columns 4–9: period (P), mass of the donor star ($m_{\rm co}$), mass of the BH ($m_{\rm BH}$), metallicity (Z), binary type (i.e. PB or EB) and Eddington luminosity ($L_{\rm Edd}$) of the best-matching simulations, respectively.
We show all the best-matching simulations with $|\Delta_{\rm V}| \leq 0.50$, $|\Delta_{\rm B-V}| \leq 0.20$ and $L_{\rm Edd} \geq 0.1\, L_{\rm X,\,max}$ (the adopted values of $L_{\rm X,\,max}$ are in Table 6). The best-matching simulations are listed in order of decreasing $L_{\rm Edd}$. See the text for details.

are matched by both RLO-PBs and RLO-EBs, the RLO-EBs always have the highest $L_{\rm Edd}$ (because they host more massive BHs). Thus, the RLO-EBs have the advantage that they do not require an exceedingly high super-Eddington factor in these three cases.

If we require not only a good matching between observed and simulated optical counterparts, but also that $L_{\rm Edd} \geq L_{\rm X,\,max}/3$ (i.e. only a mild super-Eddington factor[5]), then Ho IX X-1, NGC 1313 X-2, IC 342 X-1 and (marginally) NGC 5204 X-1 can be matched only by simulated RLO-MSBHs. The mass of the best-matching MSBHs is in the $25-77$ M$_\odot$ range. In the following, we focus on these four sources.

HO IX X-1

In the case of Ho IX X-1, a MSBH accretor is particularly favored by the high observed X-ray luminosity ($L_{\rm X,\,max} = 2.8 \times 10^{40}$ erg s^{-1}). The best-matching RLO binary[6] hosts a MSBH with $m_{\rm BH} = 77.3$ M$_\odot$, but has a metallicity much lower than the observed metallicity of Ho IX ($Z \sim 0.4$ Z$_\odot$, Table 6).

NGC 1313 X-2

The counterpart of NGC 1313 X-2 is particularly well matched by a simulated RLO-MSBH not only for the high observed X-ray luminosity ($L_{\rm X,\,max} = 0.8 \times 10^{40}$ erg s^{-1}), but also for the orbital period. In fact, the orbital period of the simulated RLO-MSBH system with $m_{\rm BH} = 25.1$ M$_\odot$ is $P = 11$ d (Table 7). NGC 1313 X-2 has an observed period either $P = 6$ d or $P = 12$ d (Liu et al. 2009), depending on the relative importance of the variations induced by X-ray irradiation and ellipsoidal modulation of the donor (Table 6). The simulated RLO-MSBH system with $P = 11$ d well matches the latter case. This is consistent with what reported by Patruno & Zampieri (2010), who found that, for an orbital period of ~ 12 days, a ~ 20 M$_\odot$ (or slightly larger) BH with a $\sim 12-15$ M$_\odot$ H-shell burning donor is compatible with the observed photometry in case of isotropic X-ray irradiation. Furthermore, the metallicity of this simulated RLO-MSBH ($Z = 0.1$ Z$_\odot$) is close to the metallicity in proximity of NGC 1313 X-2 ($Z \sim 0.1$ Z$_\odot$, Ripamonti et al. 2011 and Table 6).

IC 342 X-1

IC 342 X-1 is the observed source most significantly matched by a RLO-MSBH binary. IC 342 X-1 has an X-ray luminosity of $\sim 10^{40}$ erg s^{-1}, is close to a star-forming region, is associated with an ionized nebula and has two possible counterparts (Feng & Kaaret 2008; Cseh et al. 2012). The brightest one is consistent with a F8 to G0 Ib supergiant ($\gtrsim 10$ Myr old), if no disk emission is considered. In contrast, if the disk contribution is important, almost no constraints can be put on the companion (Feng & Kaaret 2008).

[5] We chose to focus on mildly super-Eddington systems not because we think that the considered ULXs cannot be strongly super-Eddington, but just because our code assumes Eddington-limited accretion. In a forthcoming study, we will generalize our results to super-Eddington systems.

[6] The second best-matching system for Ho IX X-1 is a RLO-PB at $Z = 0.01$ Z$_\odot$, hosts a BH with $m_{\rm BH} = 17.5$ M$_\odot$, a donor star with $m_{\rm co} = 56.0$ M$_\odot$ and has orbital period $P = 170$ d. It is not shown in Table 7, because it has $L_{\rm Edd} < 0.1\,L_{\rm X,\,max}$.

In our simulations, the best-matching models of IC 342 X-1 have $m_{\rm BH} = 21-39$ M$_\odot$, corresponding to an Eddington luminosity $L_{\rm Edd} = 3-5 \times 10^{39}$ erg s^{-1}. This requires a mild $3-4$ super-Eddington factor to match the observed $L_{\rm X,\,max}$. The companion star has a mass $m_{\rm co} = 6.7-10.7$ M$_\odot$ and is a red super-giant star (with $T_{\rm eff} \sim 3500$ K and $L \sim 1-6 \times 10^4$ L$_\odot$). The RLO phase starts at $t = 25-60$ Myr, depending on the simulation.

Most of the best-matching models are at $Z = 0.1$ Z$_\odot$, which is fairly close to the observed metallicity of IC 342 ($Z \sim 0.1-0.4$ Z$_\odot$, Table 6). Finally, in comparing the observations with our best-matching model, we do not account for intrinsic extinction. This is consistent with the observations, since Feng & Kaaret (2008) point out that the local absorption is not dominant.

NGC 5204 X-1

The best-matching RLO-MSBH system for NGC 5204 X-1 has $L_{\rm Edd} > L_{\rm X,\,max}$, while there are two RLO-LBH systems that require just a mild super-Eddington factor of ~ 4.

4.2. *Caveats and future work*

In this section, we discuss the possible issues concerning our models and the comparison with the observed ULX counterparts. First, we recall that our results hold only if the observed ULXs were born in a dense stellar association/young SC. The simulations presented in this paper do not predict the evolution of BHs that were born and evolved in low-density regions. On the other hand, most stars (and especially the most-massive stars) are believed to form in young SCs, supporting the assumption that most BHs form in young SCs. We notice that at least four sources whose counterparts are best-matched by RLO-EBs are associated with star forming regions: Ho IX X-1 and NGC 1313 X-2 are in relatively loose young SCs (Ramsey et al. 2006; Grisé et al. 2008), IC 342 X-1 is in a star forming region (Feng & Kaaret 2008) and NGC 3034 ULX5 is 0.65 arcsec away from a massive young SC (Voss et al. 2011).

A major issue is represented by infant mortality and tidal disruption of SCs. The fraction of SCs that survive gas evaporation is highly uncertain ($\approx 5-30$ per cent, e.g. Gieles & Portegies Zwart 2011). Disruption of SCs from the tidal field of the host galaxy is another important ingredient. Overall, the fraction of young SCs that survive for more than ~ 100 Myr is uncertain, but it is probably very low (~ 5 per cent, Lada & Lada 2003). The simulations presented in this paper account neither for gas evaporation nor for the galactic tidal field, which will be considered in forthcoming studies. On the other hand, we can indirectly estimate the impact of SC mortality on our results by looking at the time when EBs form ($t_{\rm bin}$) and start the RLO phase ($t_{\rm RL}$).

The underlying idea is that an EB cannot exist, if the host SC is disrupted or evaporates before the formation of the EB by dynamical exchange (i.e. before $t_{\rm bin}$). After the formation of the EB, flyby encounters with other stars can occur and they may contribute to trigger the RLO phase. On the other hand, flybys are generally much less important than exchanges, in the sense that stellar evolution is the main driver of the RLO phase in most EBs after the initial exchange. Thus, we can optimistically (pessimistically) assume that an EB enters

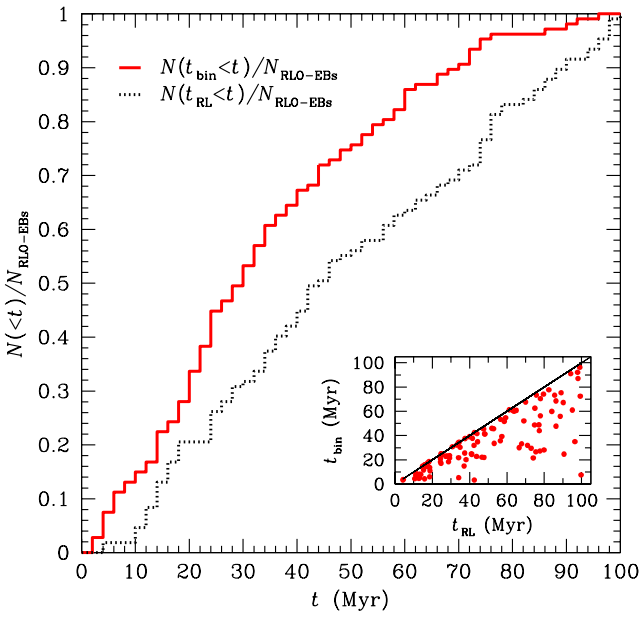

Figure 9. Red solid line ($N(t_{\rm bin} < t)/N_{\rm RLO-EBs}$): cumulative distribution of the formation times ($t_{\rm bin}$) of the EBs that will undergo RLO during the simulation, normalized to the total number of RLO-EBs ($N_{\rm RLO-EBs}$). Black dotted line ($N(t_{\rm RL} < t)/N_{\rm RLO-EBs}$): cumulative distribution of the times when the first RLO phase starts ($t_{\rm RL}$), for the simulated EBs that undergo RLO, normalized to the total number of RLO-EBs ($N_{\rm RLO-EBs}$). In the inset: $t_{\rm bin}$ versus $t_{\rm RL}$ for the simulated RLO-EBs. The solid black line marks the points with $t_{\rm bin} = t_{\rm RL}$.

the RLO phase if the SC survives for a time $t > t_{\rm bin}$ ($t > t_{\rm RL}$). Fig. 9 shows the cumulative distribution of $t_{\rm bin}$ and $t_{\rm RL}$ for all the simulated RLO-EBs, without distinguishing for metallicity. From this Figure, it is apparent that ~ 50 per cent (~ 30 per cent) of EBs that will undergo RLO have already formed (have already gone through the first RLO phase) at $t \sim 30$ Myr. These percentages indicate that the number of RLO-EBs is significantly quenched when the SC is disrupted during an early evolutionary stage. Thus, our results represent a robust upper limit to the statistics of RLO-EBs in intermediate-mass young SCs.

A further caveat is that our results are based on different realizations of a unique SC model, with the same PB fraction ($f_{\rm PB}$), total SC mass ($M_{\rm TOT}$), initial core density and concentration (see Table 1).

$f_{\rm PB}$ is a delicate ingredient of our simulations. Recent observations show that the observed binary fraction can be very high in open and young SCs ($\gtrsim 30$ per cent, with a large uncertainty, e.g. Sollima et al. 2010; Li, de Grijs & Deng 2013). On the other hand, PBs are a bottleneck for direct-summation N-body codes. Thus, most direct-summation N-body simulations do not include PBs (or include a low fraction of PBs). In our simulations, we assume $f_{\rm PB} = 0.1$, which implies (according to our definition of $f_{\rm PB}$, see Section 2.1) that 18 per cent of stars are initially in binaries.

In Appendix B, we discuss the results of test simulations with $f_{\rm PB} = 0.2$ (corresponding to 33 per cent of stars in primordial binaries). By comparing the case with $f_{\rm PB} = 0.1$ and the case with $f_{\rm PB} = 0.2$, we find that the total number of RLO-EBs remains unchanged for different values of $f_{\rm PB}$, while the total number of RLO-PBs grows about linearly with $f_{\rm PB}$. Thus, we conclude that the total number of RLO-EBs found in our simulations does not significantly depend on $f_{\rm PB}$, while the fraction of RLO-EBs with respect to the total number of RLO binaries does.

In a forthcoming study, we will focus on the impact of the main structural parameters of young SCs (e.g. total SC mass, initial core density and concentration) on the formation of X-ray binaries and other exotic binaries. We expect that the initial core density is a crucial parameter for the formation of EBs and thus for RLO-EBs, because a higher density implies a higher three-body encounter rate (e.g. Sigurdsson & Phinney 1993). The role of the total SC mass is more difficult to predict, because a larger mass means a larger number of binaries per single SC but also a longer two-body relaxation timescale. Furthermore, SCs with larger mass are less numerous in the local Universe, but might avoid infant mortality and tidal disruption (depending on the potential well of the host galaxy).

Finally, the comparison with observations presented here is still preliminary. The main limitations are that the accretion disk is assumed to be a Shakura-Sunyaev disk and the accretion rate is Eddington limited. Recent studies (e.g. Gladstone, Roberts & Done 2009; Sutton, Roberts & Middleton 2013; Middleton et al. 2014; Pintore et al. 2014) indicate that super-Eddington accretion might explain a large fraction of ULXs. A more detailed photometric analysis and modeling of disk emission at super-Eddington rates (involving a major upgrade of the Patruno & Zampieri 2010 code), combined with a new set of N-body simulations, is under way.

5. CONCLUSIONS

We simulated the evolution of 600 young SCs with different metallicity ($Z = 0.01$, 0.1 and 1 $Z_\odot$), to investigate the demographics of RLO systems powered by BHs in young SCs. The properties of the simulated young SCs match those of intermediate-mass dense young SCs in the Milky Way. Thus, the simulated young SCs are dynamically active: they undergo core collapse in ~ 3 Myr, and their evolution is driven by three-body encounters and dynamical exchanges.

In this paper, we focus on the 244 simulated BH binaries that undergo RLO (since each simulation lasts for 100 Myr, this implies a formation rate of ~ 0.004 Myr^{-1} RLO-BH binaries per SC). About 44 and 56 per cent of the simulated RLO BH binaries are RLO-EBs and RLO-PBs, respectively (Table 4). The properties of RLO-EBs are markedly different from those of RLO-PBs. RLO-EBs are generally powered by more massive BHs and start the RLO phase later than RLO-PBs (see Fig. 1). As a consequence, the mass of the donor star in RLO-EBs is ≤ 20 $M_\odot$, generally smaller than the mass of the donor star in RLO-PBs (Fig. 2). Most donor stars (~ 43 per cent) are MS stars, mainly close to the TAMS. Red giant and red super-giant branch stars are also common (~ 33 per cent, Table 5).

RLO binaries powered by MSBHs (≥ 25 $M_\odot$) are almost a sub-class of RLO-EBs, since all RLO-MSBHs but one form through dynamical exchange (Figures 3 and 4). This confirms that it is very difficult for PBs to evolve into RLO-MSBHs (see e.g. Linden et al. 2010), whereas dynamical exchanges are very efficient in pro-

ducing RLO-MSBHs (see M13).

MSBHs form mainly from the direct collapse of massive metal-poor stars, but nine MSBHs in RLO systems (corresponding to ~ 21 per cent of all the RLO-MSBHs) formed from the merger of either two stars or a BH and a star.

In this paper, we produced CMDs of the counterparts of the simulated X-ray binaries. To this purpose, we used the code by Patruno & Zampieri (2008, 2010), which couples the emission from the star with the contribution of the accretion disk. RLO-EBs and RLO-PBs form two different populations in the CMD. The sequence defined by $V \approx 24.3 - 1.6\,(B-V)$ is mainly populated by RLO-EBs (Fig. 6), whose donor stars are predominantly older and less-massive than those of RLO-PBs. In contrast, RLO-PBs are mostly associated with the bluer counterparts. In both cases, there are some remarkable exceptions (i.e. very blue RLO-EBs and very red RLO-PBs). RLO-MSBHs populate the same sequence as RLO-EBs. On the other hand, RLO-MSBHs represent the high-luminosity tail of RLO-EBs, since they populate mainly the upper envelope of this sequence (Fig. 7).

These results provide important insights to understand the observations of bright X-ray binaries in star forming regions, such as the ULXs. ULXs are associated with star forming regions and/or young SCs, and seem to anti-correlate with the metallicity of the host galaxy (e.g. Mapelli et al. 2010; Mapelli et al. 2011a). We compared the simulated RLO systems with nine of the ULX counterparts listed in G13 (Table 6). The observed counterparts populate the same regions of the CMD as the simulated ones (Fig. 6).

In particular, the counterparts of M81 X-6 and NGC 1313 X-1 are matched only by simulated RLO-PBs, the counterparts of NGC 1313 X-2, NGC 2403 X-1 and NGC 5204 X-1 can be matched by both simulated RLO-PBs and simulated RLO-EBs, while the counterparts of Ho IX X-1 and IC 342 X-1 are matched only by simulated RLO-EBs.

If we require not only a good matching between observed and simulated optical counterparts, but also that the maximum observed X-ray luminosity does not exceed the Eddington luminosity by a factor larger than three, then Ho IX X-1, NGC 1313 X-2, IC 342 X-1 and (marginally) NGC 5204 X-1 can be matched only by simulated RLO-MSBHs.

The counterpart of NGC 1313 X-2 is particularly well matched by a simulated RLO-MSBH not only for the high observed X-ray luminosity ($L_{\rm X,\,max} = 0.8 \times 10^{40}$ erg s^{-1}), but also for the simulated orbital period ($P = 11$ d, see Table 7), consistent with the observed one in case ellipsoidal modulations significantly affect the light curve (Liu et al. 2009).

The counterpart of IC 342 X-1 is the most significantly matched by a RLO-MSBH (with BH mass $m_{\rm BH} = 21 - 39$ M$_\odot$). This interpretation is supported also by recent *Chandra*, NuSTAR and XMM observations (Marlowe et al. 2014; Rana et al. 2014; Pintore et al. 2014). The donor star of the best matching systems is a relatively low-mass (6.7–10.7 M$_\odot$) red super-giant star.

Unfortunately, a robust identification of the optical counterpart was obtained only for a few ULXs (e.g. G13 and references therein). Furthermore, a measurement of the orbital period is available only for four ULXs (NGC 3034 ULX5, Kaaret et al. 2006; NGC 1313 X-2, Liu et al. 2009; CXOU J123030.3+413853 in NGC 4490, Esposito et al. 2013; and M101 X-1, Liu et al. 2013). Besides, in our study we did not consider intrinsic extinction, which is an additional factor of uncertainty. In addition, our code (Patruno & Zampieri 2010) is based on a Shakura-Sunyaev disk model, and assumes that any mass transfer in excess of the Eddington limit is expelled from the system. Thus, it is very difficult to make a robust comparison between data and models.

In addition, ULXs are very peculiar and rare objects (an occurrence rate of less than one ULX per galaxy has been found in the catalog by Swartz et al. 2011). Our simulations represent a statistically limited sample: 600 young SCs are approximately the young SC content of a single starburst galaxy. Furthermore, we considered only a relatively small fraction of PBs, we simulated different realizations of a single SC model (with the same total mass, virial radius and concentration), and we did not account for gas evaporation and for the tidal field of the host galaxy. Thus, a larger sample of $N-$body simulations (including prescriptions for the missing ingredients) is necessary to obtain a complete statistical description of RLO systems in young SCs and to compare them with observed X-ray sources.

Bearing these caveats in mind, our simulations show (for the first time in a self-consistent way) that RLO-MSBHs in young SCs can reproduce the optical properties of observed ULX counterparts. This result is very promising, because a growing number of observations suggest that (some) ULXs might be powered by MSBHs: this scenario is consistent with the observed anti-correlation between ULXs and metallicity of the host galaxy (Mapelli et al. 2009; Mapelli et al. 2010; Mapelli et al. 2011a; Prestwich et al. 2013), with the measured mass function of M 101 ULX-1 (Liu et al. 2013), and with the recent radio observations of Holmberg II X-1 (Cseh et al. 2014).

ACKNOWLEDGMENTS

We thank the anonymous referee for their comments, which significantly improved the paper. We also thank Jeannette Gladstone and Nathan Leigh for their invaluable comments, and Alessia Gualandris, Alessandro Bressan and Emanuele Ripamonti for useful discussions. We made use of the STARLAB (version 4.4.4) public software environment and of the SAPPORO library (Gaburov, Harfst & Portegies Zwart 2009). We thank the developers of STARLAB, and especially its primary authors (P. Hut, S. McMillan, J. Makino, and S. P. Zwart). We thank the authors of SAPPORO, and in particular E. Gaburov, S. Harfst and S. Portegies Zwart. We acknowledge the CINECA Award N. HP10CXB7O8, HP10C894X7, HP10CGUBV0, HP10CP6XSO and HP10C3ANJY for the availability of high performance computing resources and support. The simulations were run on the graphics processing unit (GPU) clusters IBM-PLX and EURORA at CINECA. MM and LZ acknowledge financial support from the Italian Ministry of Education, University and Research (MIUR) through grant FIRB 2012 RBFR12PM1F, and from INAF through grant PRIN-2011-1. MM acknowledges financial support from

CONACyT through grant 169554.

APPENDIX

A. THE SAMPLE OF ULX COUNTERPARTS

The most recent and homogeneous sample of optical ULX counterparts has been reported by G13. Of the 33 ULXs observed with both *HST* and *Chandra*, and studied in G13, nine have no visible counterparts, and two were found to lie too close to the nucleus of the host galaxy to be classified as ULXs. The remaining 22 ULXs have at least one detected possible counterpart with *HST*. Among them, we selected nine ULXs (see Table 6), according to the following criteria.

We selected the six ULXs (M81 X-6, Ho IX X-1, NGC 1313 X-1, NGC 1313 X-2, IC 342 X-1 and NGC 3034 ULX5) with *HST* data in the F555W and in the F435W filters (approximately corresponding to the Johnson V and B filters, which are implemented in the code by Patruno & Zampieri 2010). In addition, we selected the three ULXs (NGC 2403 X-1, M83 XMM1 and NGC 5204 X-1) for which there are *HST* data in both the F435W and the F606W filter (corresponding to a wide V filter), but no observations with the F555W filter. Three of the six ULXs with *HST* data in both the F555W and the F435W filters have also observations in the F606W filter (M81 X-6, NGC 1313 X-1 and IC 342 X-1). As a proxy to the transformation between different filters, for the three sources that lack F555W data we convert the F606W magnitude into a F555W magnitude using the average shift between the F555W and F606W filters, determined from the counterparts with both measurements.

Five of the nine considered sources (Ho IX X-1, NGC 1313 X-2, IC 342 X-1, NGC 5204 X-1 and NGC 3034 ULX5) have multiple possible counterparts in the *Chandra* error box. In particular, both IC 342 X-1 and NGC 5204 X-1 have two possible counterparts in the *Chandra* error box and each of them has *HST* data in both V and B. In Figures 6 and 7, we plot only the counterpart of IC 342 X-1 and that of NGC 5204 X-1 that were labelled as 1 in Table 4 of G13. We analyzed also the counterparts of IC 342 X-1 and of NGC 5204 X-1 that were labelled as 2, but they do not match any simulated systems.

Both NGC 1313 X-2 and NGC 3034 ULX5 have two possible counterparts in the *Chandra* error box, but only one of the two was detected in both V and B. Thus, for both NGC 1313 X-2 and NGC 3034 ULX5, we consider only the counterpart which has been detected in both V and B. Furthermore, object 1 is the most likely counterpart of NGC 1313 X-2, based on the identification of the He II 4686 Å emission line in the spectrum (Grisé et al. 2008) and on the accurate *Chandra* and *HST* astrometry (Liu et al. 2007). In addition, object 2 might be an artifact of data analysis (Jeannette Gladstone, private communication).

Ho IX X-1 has three possible counterparts in the *Chandra* error box: counterparts 1 and 3 have F435W and F555W data, while counterpart 2 was detected only in the F330W filter (because the data considered in G13 do not have the spatial resolution to separate it from source 1 in any band but F330W). In Figures 6 and 7, we plot only counterpart 1 of Ho IX X-1. We analyzed also counterpart 3, but it does not match any simulated system. Furthermore, object 1 is the most likely counterpart of Ho IX X-1, based on the identification of the He II 4686 Å emission line in the spectrum (Roberts et al. 2011).

Table 8
Most relevant initial conditions of 100 runs with $f_{\rm PB} = 0.2$.

Parameter	Values
W_0	5
N_*	5640
$r_{\rm c}$ (pc)	0.4
c	1.03
IMF	Kroupa (2001)
$m_{\rm min}$ ($M_\odot$)	0.1
$m_{\rm max}$ ($M_\odot$)	150
Z ($Z_\odot$)	0.1
$f_{\rm PB}$	0.2

Note. — *Notes.* The symbols are the same as in Table 1. In each simulated SC, there are initially 4700 CMs, among which 940 are designated as 'binaries' and 3760 are 'single stars'. Thus, 1880 stars per SC are initially in binaries.

Table 9
Comparison of the simulated RLO systems in SCs with different PB fraction.

$f_{\rm PB}$	RLO	RLO-PBs	RLO-EBs	RLO-MSBHs	RLO-LBHs
0.2	56 ± 7	39 ± 6	17 ± 4	6 ± 2	50 ± 7
0.1	41 ± 5	22.5 ± 3	18.5 ± 3	9 ± 2	32 ± 4

Note. — *Notes.* $f_{\rm PB}$ (column 1): PB fraction in the simulates SCs; RLO (column 2): number of all simulated RLO systems per SC; RLO-PBs (column 3): number of PBs that undergo RLO; RLO-EBs (column 4): number of EBs that undergo RLO; RLO-MSBHs (column 5): number of RLO systems powered by MSBHs; RLO-LBHs (column 6): number of RLO systems powered by BHs with mass<25 $M_\odot$ for different metallicities and in total.
Both the SCs with $f_{\rm PB} = 0.1$ and the SCs with $f_{\rm PB} = 0.2$ have metallicity $Z = 0.1$ $Z_\odot$. The tabulated numbers for the SCs with $f_{\rm PB} = 0.1$ come from Table 4 but have been divided by two to match the number of runs with $f_{\rm PB} = 0.2$ (we ran 200 simulations with $Z = 0.1$ $Z_\odot$ and $f_{\rm PB} = 0.1$ and 100 simulations with $Z = 0.1$ $Z_\odot$ and $f_{\rm PB} = 0.2$). All SCs have been simulated for 100 Myr.
The tabulated uncertainties are Poissonian errors.

B. THE IMPACT OF THE BINARY FRACTION

In this Appendix, we discuss the impact of the PB fraction on our results. In the runs presented in the main text, we have assumed $f_{\rm PB} = 0.1$, which means that 18 per cent of the simulated stars are in binaries at the beginning of the simulation. Recent observations (e.g. Sollima et al. 2010; Li, de Grijs & Deng 2013) indicate that the binary fraction in young SCs may be significantly higher. However, high PB fractions are a severe bottleneck for direct-summation N-body simulations. Thus, it is very difficult to obtain a good statistical sample of simulated young SCs with a high PB fraction.

In order to quantify the impact of the binary fraction on our results, we have run an additional sample of 100 young SCs with metallicity $Z = 0.1$ $Z_\odot$ and PB fraction $f_{\rm PB} = 0.2$. This means that ~ 33 per cent of the stars are members of a binary system at the beginning of the simulation.

To compare SCs with the same relevant dynamical timescales (e.g. initial two-body relaxation timescales), we imposed that the SCs with $f_{\rm PB} = 0.2$ have the same total mass ($M_{\rm TOT} \sim 3500$ $M_\odot$) and virial radius (1 pc) as the SCs with $f_{\rm PB} = 0.1$. More details about the initial conditions of the SCs with $f_{\rm PB} = 0.2$ are given in Table 8.

Table 9 compares the main statistical properties of

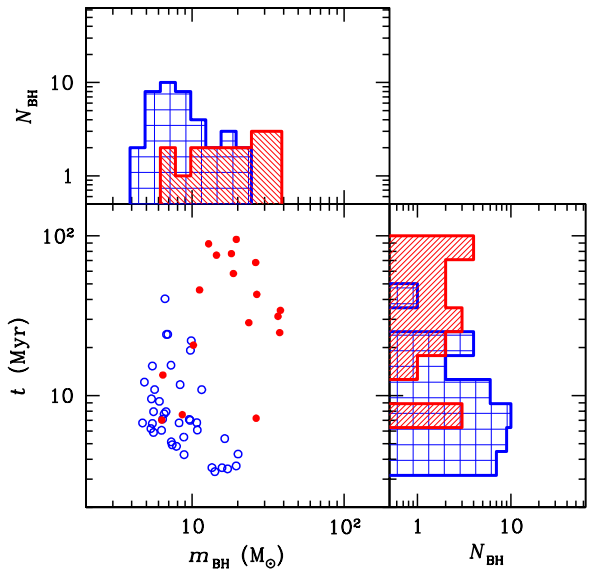

Figure 10. Main window: mass of the BHs that power simulated RLO systems versus the time when the RLO phase starts for the 100 runs with $f_{PB} = 0.2$ and $Z = 0.1$ $Z_\odot$. Red filled circles: RLO-EBs; blue open circles: RLO-PBs. The marginal histograms show the distribution of the masses of BHs that power RLO systems and the distribution of the times when the RLO phase starts ($t = 0$ is the beginning of the simulation). In both marginal histograms, the red hatched histogram (blue cross-hatched histogram) refers to RLO-EBs (RLO-PBs).

RLO systems in SCs with $f_{PB} = 0.2$ and with $f_{PB} = 0.1$, respectively. The number of RLO systems in SCs with $f_{PB} = 0.2$ is considerably higher (by a factor of ~ 1.4) than that of RLO systems in SCs with $f_{PB} = 0.1$. This is due to the much larger number of RLO-PBs in the SCs with higher f_{PB}: the number of RLO-PBs in SCs with $f_{PB} = 0.2$ is a factor of ~ 1.7 higher than that of RLO-PBs in SCs with $f_{PB} = 0.1$.

In contrast, the number of RLO-EBs in the runs with $f_{PB} = 0.2$ remains substantially unchanged (see column 4 of Table 9) with respect to the runs with $f_{PB} = 0.1$. The number of RLO-MSBHs in the runs with $f_{PB} = 0.2$ is fairly consistent with that of RLO-MSBHs in the runs with $f_{PB} = 0.1$, within Poissonian uncertainties.

Fig. 10 shows the distribution of BH masses and that of the times when the RLO phase starts for RLO-PBs and RLO-EBs in the SCs with $f_{PB} = 0.2$. RLO-EBs tend to host more massive BHs and to start the RLO phase later than RLO-PBs. This is fairly consistent with the results that we obtained for the SCs with $f_{PB} = 0.1$ (Figures 1 and 2).

In conclusion, the main effect of including a higher PB fraction in the simulated SCs is that the absolute number of RLO-PBs increases significantly. In contrast, the number of RLO-EBs is not affected by the initial binary fraction. We expect that the number of RLO-EBs depends more on the structural properties of the SCs (e.g. the central density and the timescale for core collapse). The other main results of this paper (i.e. the fact that RLO-EBs statistically host more massive BHs/less massive donor stars and start the RLO phase later than RLO-PBs) are not affected by the PB fraction.

REFERENCES

Aarseth S. J., Hills J. G. 1972, A&A, 21, 255
Abolmasov P. K., Swartz D. A., Fabrika S., Ghosh K. K., Sholukhova O., Tennant A. F. 2007, ApJ, 668, 124
Bastian N. 2008, MNRAS, 390, 759
Belczynski K., Kalogera V., Zezas A., Fabbiano G. 2004a, ApJ, 601, L147
Belczynski K., Sadowski A., Rasio F. A. 2004b, ApJ, 611, 1068
Belczynski K., Kalogera V., Rasio F. A., Taam R. E., Zezas A., Bulik T., Maccarone Th. J., Ivanova N. 2008, ApJS, 174, 223
Belczynski K., Bulik T., Fryer C. L., Ruiter A., Valsecchi F., Vink J. S., Hurley J. R. 2010, ApJ, 714, 1217
Berghea C. 2009, *Ultraluminous X-ray sources and their Environment*, PhD thesis, `http://students.cua.edu/79berghea/papers/dissertation.pdf`
Berghea C. T., Dudik R. P., Tincher J., Winter L. M. 2013, ApJ, 776, 100
Blecha L., Ivanova N., Kalogera V., Belczynski K., Fregeau J., Rasio F. 2006, ApJ, 642, 427
Bodaghee A., Tomsick J. A., Rodriguez J., James J. B. 2012, ApJ, 744, 108
Bressert E. et al. 2010, MNRAS, 409, L54
Casella P., Ponti G., Patruno A., Belloni T., Miniutti G., Zampieri L. 2008, MNRAS, 387, 1707
Coleiro A., Chaty S. 2013, ApJ, 764, 185
Colpi M., Mapelli M., Possenti A. 2003, ApJ, 599, 1260
Copperwheat Ch., Cropper M., Soria R., Wu K. 2005, MNRAS, 362, 79
Copperwheat C., Cropper M., Soria R., Wu K. 2007, MNRAS, 376, 1407
Cseh D., Corbel S., Kaaret P., Lang C., Grisé F., Paragi Z., Tzioumis A., Tudose V., Feng H. 2012, ApJ, 749, 17
Cseh D., Kaaret P., Corbel S., Grisé F., Lang C., Körding E., Falcke H., Jonker P. G., Miller-Jones J. C. A., Farrell S., et al. 2014, MNRAS, 439, L1
Davies M. B. 1995, MNRAS, 276, 887
de Vaucouleurs G., de Vaucouleurs A., Corwin H. G. Jr., Buta R. J., Paturel G., Fouque P. 1991, *Third Reference Catalogue of Bright Galaxies*, Springer-Verlag Berlin Heidelberg New York
Dias W. S., Alessi B. S., Moitinho A., Lépine J. R. D. 2002, A&A, 389, 871
Downing J. M. B., Benacquista M. J., Giersz M., Spurzem R. 2011, MNRAS, 416, 133
Dray L. M. 2006, MNRAS, 370, 2079
Esposito P., Israel G. L., Sidoli L., Mapelli M., Zampieri L., Motta S. E. 2013, MNRAS, 436, 3380
Feng H., Kaaret P. 2008, ApJ, 675, 1067
Feng H., Kaaret P. 2010, ApJ, 712, L169
Fryer Ch. L. 1999, ApJ, 522, 413
Fryer Ch. L., Belczynski K., Wiktorowicz G., Dominik M., Kalogera V., Holz D. E. 2012, ApJ, 749, 91
Gaburov E., Harfst S., Portegies Zwart S. 2009, New Astronomy, 14, 630
Gaburov E., Lombardi J. C. Jr., Portegies Zwart S. 2010, MNRAS, 402, 105
Gieles M., Portegies Zwart S. F. 2011, MNRAS, 410, L6
Gieles M., Moeckel N., Clarke C. J. 2012, MNRAS, 426, L11
Gladstone J. C., Roberts T. P., Done Ch. 2009, MNRAS, 397, 1836
Gladstone J. C., Copperwheat Ch., Heinke C. O., Roberts T. P., Cartwright T. F., Levan A. J., Goad M. R. 2013, ApJS, 206, 14
Goad M. R., Roberts T. P., Knigge C., Lira P. 2002, MNRAS, 335, L67
Goddard Q. E., Bastian N., Kennicutt R. C. 2010, MNRAS, 405, 857
Goswami S., Kiel P., Rasio F. A. 2014, ApJ, 781, 81
Grisé F., Pakull M. W., Soria R., Motch C., Smith I. A., Ryder S. D., Böttcher M. 2008, A&A, 486, 151
Grisé F., Kaaret P., Pakull M. W., Motch C. 2011, ApJ, 734, 23
Grisé F., Kaaret P., Corbel S., Feng H., Cseh D., Tao L. 2012, ApJ, 745, 123
Gvaramadze V. V., Weidner C., Kroupa P., Pflamm-Altenburg J. 2012, MNRAS, 424, 3037
Hamann W.-R., Koesterke L. 1998, A&A, 335, 1003
Hartman J. W. 1997, A&A, 322, 127

Heger A., Fryer C.L., Woosley S.E., Langer N., Hartmann D.H. 2003, ApJ, 591, 288
Heggie D. C. 1975, MNRAS, 173, 729
Heggie D. C., Hut P. 1993, ApJS, 85, 347
Hillenbrand L. A., Hartmann L. W. 1998, ApJ, 492, 540
Hills J. G. 1975, AJ, 80, 809
Hills J. G. 1976, MNRAS, 175, 1
Hills J. G., Fullerton L. W. 1980, AJ, 85, 1281
Hills J. G. 1989, AJ, 97, 222
Hills J. G. 1991, AJ, 102, 704
Hills J. G. 1992, AJ, 103, 1955
Humphreys R. M., Davidson K. 1994, Astronomical Society of the Pacific, Publications, 106, 1025
Hurley J. R., Pols O. R., Tout C. A. 2000, MNRAS, 315, 543
Hurley J. R., Tout C. A., Pols O. R. 2002, MNRAS, 329, 897
Kaaret P., Prestwich A. H., Zezas A., Murray S. S., Kim D.-W., Kilgard R. E., Schlegel E. M., Ward M. J. 2001, MNRAS, 321, L29
Kaaret P., Alonso-Herrero A., Gallagher J. S., Fabbiano G., Zezas A., Rieke M. J. 2004, MNRAS, 348, L28
Kaaret P., Simet M. G., Lang C. C. 2006, ApJ, 646, 174
Kaaret P., Feng H. 2013, ApJ, 770, 20
Kharchenko N. V., Piskunov A. E., Schilbach E., Röser S., Scholz R.-D. 2012, A&A, 543, 156
Kharchenko N. V., Piskunov A. E., Schilbach E., Röser S., Scholz R.-D. 2013, A&A, 558, 53
King I. R. 1966, AJ, 71, 64
Kroupa P. 2001, MNRAS, 322, 231
Kuhn M. A., Baddeley A., Feigelson E. D., Getman K. V., Broos P. S., Townsley L. K., Povich M. S., Naylor T., King R. R., Busk H. A., Luhman K. L. 2012, arXiv:1208.3492, to appear in The Labyrinth of Star Formation, (eds.) D. Stamatellos, S. Goodwin, and D. Ward-Thompson, Springer, in press
Lada Ch. J., Lada E. A. 2003, ARA&A, 41, 57
Leigh N. W. C., Geller A. M. 2013, MNRAS, 432, 2474
Li C., de Grijs R., Deng L. 2013, MNRAS, 436, 1497
Linden T., Kalogera V., Sepinsky J. F., Prestwich A., Zezas A., Gallagher J. 2010, ApJ, 725, 1984
Liu J.-F., Bregman J., Seitzer P. 2004, ApJ, 602, 249
Liu J.-F., Bregman J., Miller J., Kaaret P. 2007, ApJ, 661, 165
Liu J., Bregman J. N., McClintock J. E. 2009, ApJ, 690, L39
Liu J., Bregman J. N., Bai Y., Justham S., Crowther P. 2013, Nature, 503, 500
Madhusudhan N., Justham S., Nelson L., Paxton B., Pfahl E., Podsiadlowski Ph., Rappaport S. 2006, ApJ, 640, 918
Madhusudhan N., Rappaport S., Podsiadlowski Ph., Nelson L. 2008, ApJ, 688, 1235
Makarova L. N., Grebel E. K., Karachentsev I. D., Dolphin A. E., Karachentseva V. E., Sharina M. E., Geisler D., Guhathakurta P., Hodge P. W., Sarajedini A., Seitzer P. 2002, A&A, 396, 473
Mapelli M., Colpi M., Possenti A., Sigurdsson S. 2005, MNRAS, 364, 1315
Mapelli M., Colpi M., Zampieri L. 2009, MNRAS, 395L, 71
Mapelli M., Ripamonti E., Zampieri L., Colpi M., Bressan A. 2010, MNRAS, 408, 234
Mapelli M., Ripamonti E., Zampieri L., Colpi M. 2011a, AN, 332, 414
Mapelli M., Ripamonti E., Zampieri L., Colpi M. 2011b, MNRAS, 416, 1756
Mapelli M., Zampieri L., Ripamonti E., Bressan A. 2013, MNRAS, 429, 2298 (M13)
Mapelli M., Bressan A. 2013, MNRAS, 430, 3120
Marlowe H., Kaaret P., Lang C., Feng H., Grisé F., Miller N., Cseh D., Corbel S., Mushotzky R. F., 2014, MNRAS, accepted, arXiv:1407.6254
Middleton, M. J., Walton, D. J., Roberts, T. P., Heil, L. 2014, MNRAS, 438, L51
Mucciarelli P., Zampieri L., Treves A., Turolla R., Falomo R. 2007, ApJ, 658, 999
Nelemans G., Yungelson L. R., Portegies Zwart S. F., Verbunt F. 2001, A&A, 365, 491
Pakull M. W., Mirioni L. 2002, astro-ph/0202488
Parker R. J., Goodwin S. P. 2007, MNRAS, 380, 1271
Patruno A., Portegies Zwart S., Dewi J., Hopman C. 2006, MNRAS, 370, L6
Patruno A., Zampieri L. 2008, MNRAS, 386, 543
Patruno A., Zampieri L. 2010, MNRAS, 403, L69
Pfalzner S. 2009, A&A, 498, L37
Pintore F., Zampieri L. 2012, MNRAS, 420, 1107
Pintore F., Zampieri L., Wolter A., Belloni T. 2014, MNRAS, 439, 3461
Podsiadlowski Ph., Rappaport S., Pfahl E. D. 2002, ApJ, 565, 1107
Podsiadlowski Ph., Rappaport S., Han Z. 2003, MNRAS, 341, 385
Porras A., Christopher M., Allen L., Di Francesco J., Megeath S. Th., Myers Ph. C. 2003, AJ, 126, 1916
Portegies Zwart S. F., Verbunt F. 1996, A&A, 309, 179
Portegies Zwart S. F., Verbunt F., Ergma E. 1997, A&A, 321, 207
Portegies Zwart S. F., McMillan S. L. W., Hut P., Makino J. 2001, MNRAS, 321, 199
Portegies Zwart S. F., McMillan S. L. W. 2002, ApJ, 576, 899
Portegies Zwart S. F., McMillan S. L. W., Makino J. 2007, MNRAS, 374, 95
Portegies Zwart S. F., McMillan S. L. W., Gieles M. 2010, ARA&A, 48, 431
Poutanen J., Fabrika S., Valeev A. F., Sholukhova O., Greiner J. 2013, MNRAS, 432, 506
Prestwich A. H., Tsantaki M., Zezas A., Jackson F., Roberts T. P., Foltz R., Linden T., Kalogera V. 2013, ApJ, 769, 92
Ramsey C. J., Williams R. M. Gruendl R. A., Chen C.-H. R., Chu Y.-H., Wang Q. D. 2006, ApJ, 641, 241
Rana V. et al. 2014, ApJ, submitted, arXiv:1401.4637
Rangelov B., Chandar R., Prestwich A., Whitmore B. C. 2012, ApJ, 758, 99
Rappaport S. A., Podsiadlowski Ph., Pfahl E. 2005, MNRAS, 356, 401
Ripamonti E., Mapelli M., Zampieri L., Colpi M. 2011, AN, 332, 418
Roberts T. P., Gladstone J. C., Goulding A. D., Swinbank A. M., Ward M. J., Goad M. R., Levan A. J. 2011, AN, 332, 398
Sepinsky J., Kalogera V., Belczynski K. 2005, ApJ, 621L, 37
Sigurdsson S., Phinney E. S. 1993, ApJ, 415, 631
Sigurdsson S., Phinney E. S. 1995, ApJS, 99, 609
Silva-Villa E., Larsen S. S. 2010, A&A, 516, 10
Sollima A., Carballo-Bello J. A., Beccari G., Ferraro F. R., Fusi Pecci F., Lanzoni B. 2010, MNRAS, 401, 577
Soria R., Cropper M., Pakull M., Mushotzky R., Wu K. 2005, MNRAS, 356, 12
Sutton, A. D., Roberts, T. P., Middleton, M. J. 2013, MNRAS, 435, 1758
Swartz D. A., Tennant A. F., Soria R. 2009, ApJ, 703, 159
Swartz D. A., Soria R., Tennant A. F., Yukita M. 2011, ApJ, 741, 49
Tao L., Feng H., Grisé F., Kaaret Ph. 2011, ApJ, 737, 81
Terashima Y., Inoue H., Wilson A. S. 2006, ApJ, 645, 264
van der Hucht K. A. 1991, in 'Wolf-Rayet Stars and Interrelations with Other Massive Stars in Galaxies': Proceedings of the 143rd Symposium of the International Astronomical Union. Edited by Karel A. van der Hucht and Bambang Hidayat. International Astronomical Union. Symposium no. 143, Kluwer Academic Publishers, Dordrecht, p.19
Vink J. S., de Koter A., Lamers H. J. G. L. M. 2001, A&A, 369, 574
Vink J. S., de Koter A. 2005, A&A, 442, 587
Voss R., Nielsen M. T. B., Nelemans G., Fraser M., Smartt S. J. 2011, MNRAS, 418, L124
Winter L. M., Mushotzky R. F., Reynolds C. S. 2006, ApJ, 649, 730
Zampieri L., Mucciarelli P., Falomo R., Kaaret P., Di Stefano R., Turolla R., Chieregato M., Treves A. 2004, ApJ, 603, 523
Zampieri L., Roberts T. 2009, MNRAS, 400, 677
Zezas A., Fabbiano G., Rots A. H., Murray S. S. 2002, ApJ, 577, 710
Zuo Z.-Y., Li X.-D. 2010, MNRAS, 405, 2768